論文 / 著書情報
Article / Book Information

題目(和文)	惑星移動と原始惑星形成
Title(English)	Protoplanet formation with the effect of type-I migration
著者(和文)	小南淳子
Author(English)	
出典(和文)	学位:博士（理学）, 学位授与機関:東京工業大学, 報告番号:甲第5975号, 授与年月日:2005年3月26日, 学位の種別:課程博士, 審査員:井田茂
Citation(English)	Degree:Doctor of Science, Conferring organization: Tokyo Institute of Technology, Report number:甲第5975号, Conferred date:2005/3/26, Degree Type:Course doctor, Examiner:
学位種別(和文)	博士論文
Type(English)	Doctoral Thesis

Protoplanet Formation with the Effect of Type-I Migration

Junko Kominami

Contents

Abstract

We have performed N-body simulations on the stage of protoplanet formation from planetesimals, taking into account so-called "type-I migration", and damping of orbital eccentricities and inclinations, as a result of tidal interaction with a gas disk without gap formation. One of the most serious problems in formation of terrestrial planets and Jovian planet cores is that the orbital migration time scale predicted by the linear theory is shorter than their formation time scales and disk lifetime. Type-I migration moves to "type-II migration", when a gap opens in the gas disks near the orbit of a protoplanet, with which the migration time scale is comparable with disk life time. However, mass of the terrestrial planets and Jovian planet cores may be insufficient to open up a gap in the gas disks. In this paper, we focus on type-I migration. Several factors can alter the migration time scale: 1) the gap opening in the planetesimal disk through gravitational perturbations from the protoplanet, and 2) the effect from other protoplanets. The effect 1) is as follows. The planetesimal disk with a gap exerts torque on the protoplanet to slow down the migration as in the case of "type-II migration" in the gas disk. It is expected that gap opening is easier in the planetesimal disk than in the gas disk. The effect 2) is as follows. The linear theory of type-I migration assumes a protoplanet being alone in a gas disk. However, formation of comparable-sized multiple protoplanets ("oligarchic growth") is expected. The interaction with other protoplanets has potential to alter the migration speed. In order to investigate the effect 1), we carried out N-body simulations of the planetesimal disk with a protoplanet seed in order to clarify how much retardation can be induced by the planetesimal disk and how long such retardation can last. Gravitational interactions and physical collisions of every body are included. In order to include type-I migration, the toque exerted by the gas disk is given in the form of forces in equation of motion according to the results from the linear theory. We simulated six cases with different migration speed. We found that in all of our simulations, a clear gap is not maintained for more than 10^5 years in the planetesimal disk, so that the type-I

migration does not slow down. For very fast migration, a gap cannot be created. For migration slower than some critical speed, a gap is formed. After the formation of the gap, since we allow the accretion of the planetesimals, gravitational perturbation of the planetesimals eventually becomes strong enough for diffusion of the planetesimals into the vicinity of the protoplanets. After the gap is destroyed, the close encounters with the planetesimals make the protoplanet migration rather faster. Thus, the migration time scale is not altered by the torque from the planetesimal disk, regardless of the migration speed. In order to investigate the effect 2), we performed another series of N-body simulations with a wider range of the disk, starting from the planetesimals without the protoplanet seeds. We assume the disk gas decreases exponentially with time as well. The parameters are the gas depletion time scale and the initial disk surface density. We found out that the migration and the accretion process of a runaway protoplanet are not affected by the other protoplanets and planetesimals placed inner and outer regions of its orbit. We also derived a formula for expressing the time evolution of solid surface density as a function of depletion time scale, initial gas surface density, and semimajor axis, which is in good agreement with the N-body simulations. The simulations show that the evolution can be expressed with the analytical formula that considers only one body migrating in a gas disk. The formula gives the final surface density of solid material (protoplanets, planetesimals) after the gas depletion as a function of depletion time scale ,initial gas and dust surface densities. Using the analytical formula and the N-body simulation results, we also discuss the relation between the final planets and the initial planetesimal disks with various gas to dust ratio. In order to retain a solid surface density of the minimum mass solar nebula, it is necessary either to make the gas depletion time scale to $\sim 10^5$ years, to retard the migration speed at least by several times from that given by linear theory (due to effects such as turbulence and radiative transfer) for gas depletion time scale of $\sim 10^6$-10^7 years or to adopt the gas to dust ratio ~ 10 (gas poor) in the disk when the planetesimal accretion starts. The low gas to dust ratio is preferred for habitable planet formation as well. We also found out that if type-I migration is considered, disk's solid component profile becomes flatter than MMSN after the gas depletion. The inner region of the disk is depleted significantly. This result is consistent with our Solar system, because no planet exists inside Mercury, and may also apply to other planetary systems as well.

Chapter 1

Introduction

1.1 Planet Formation Scenario

Planets are formed through the accretion of smaller bodies, called planetesimals. The $\sim$ km sized planetesimals coagulate and runaway accretion takes place to form runaway bodies (e.g., Greenberg et al.1978, Wetherill and Stewart 1989, 1993, Spaute et al. 1991, Barge and Pellat 1991, Kokubo and Ida 1996, Inaba et al. 2001). Such runaway bodies continue to grow oligarchicly and reach isolation mass, which is about the size of the Mars in the cases of the minimum mass solar nebula (MMSN)(Hayashi 1981), and form about $\sim$ 20 protoplanets in the terrestrial planet region (Kokubo and Ida 1998, 2000, Weidenschilling et al. 1997). The protoplanets that reach the isolation mass become stable temporarily. However, their orbits become unstable after a certain period, and they start to coagulate through giant impacts and form terrestrial planets (e.g., Chambers and Wetherill 1998, Agnor et al. 1999, Kominami and Ida 2002).

1.2 Effect from the Gas Disk

Since the planet formation takes place in an abundant gas disk except in the final stage, the bodies suffer the orbital changes due to the aerodynamical gas drag (Adachi et al. 1976) and the disk-planet interaction (Goldreich and Tremaine 1979, 1980). As the planets grow, they tidally excite density waves in the gas disks. The recoil of the wave excitation damps the bodies' eccentricities and inclinations (Shu et al. 1983, Ward 1988, 1993, Artymowicz

1993, 1994, Ward and Hahn 1994, Tanaka and Ward 2004). The excitation also exerts a net torque on the bodies and usually takes away the angular momentum of the bodies (Ward 1986, Korycansky and Pollack 1993, Tanaka et al. 2002). In this paper, we will call the damping due to this tidal interaction with gas disks as "gravitational drag". This type of migration is known as "type-I migration". Highly eccentric and inclined orbits, which are acquired during the giant impact stage, can be damped by the wave excitation in the residual disk (Kominami and Ida 2002, Agnor and Ward 2002).

The orbital elements of small planetesimals are mainly damped by the aerodynamical gas drag. When a body is larger than lunar size, the gravitational drag dominates the damping (Ward 1993). Since the isolated protoplanets are about Mars-sized in MMSN, the disk-planet interaction has large effect on formation of protoplanets. The migration time scale for a Mars-sized planet at 1AU is estimated to be 7×10^5 years (Tanaka and Ward 2004). Since this time scale is comparable to or shorter than the depletion time scale of disk gas, the protoplanets would suffer large inward migration. It is more difficult for the Jovian planets' cores to survive the migration. For example, the migration time scale for a core with $5M_\oplus$ at 5 AU is 1.6×10^5 years, which is much shorter than the formation time scale of the core (Kokubo and Ida 2002, Inaba et al. 2003). For the core to be transformed into a gas giant planet, it must acquire a mass of this size before disk gas depletion. Figure 1.1 shows in which disk, with what depletion time scale, planets with isolation mass at 1AU can survive, assuming a fixed gas to dust ratio, $\Sigma_{\rm g}/\Sigma_{\rm s} = \Sigma_{\rm g,SN}/\Sigma_{\rm s,SN}$, where $\Sigma_{\rm s}$ and $\Sigma_{\rm g}$ are the solid and gas surface densities of the disk respectively, and $\Sigma_{\rm s,SN}$ and $\Sigma_{\rm g,SN}$ are those in MMSN, defined by (Hayashi 1981)

$$\Sigma_{\rm s,SN} = 7.1 f_{\rm ice} \left(\frac{a}{1\rm AU}\right)^{-3/2} \quad ({\rm g/cm^2}), \quad \Sigma_{\rm g,SN} = 1.7 \times 10^3 \left(\frac{a}{1\rm AU}\right)^{-3/2} \quad ({\rm g/cm^2}). \quad (1.1)$$

Since there is an ice boundary ($\sim$ 3 AU in Solar system) in the disk, $f_{\rm ice}$ is 1.0 at $a < 3.0$AU and 4.0 at $a > 3.0$AU. The line is drawn by equating $\tau_{\rm grav,mig}$ (2.12) with disk gas depletion

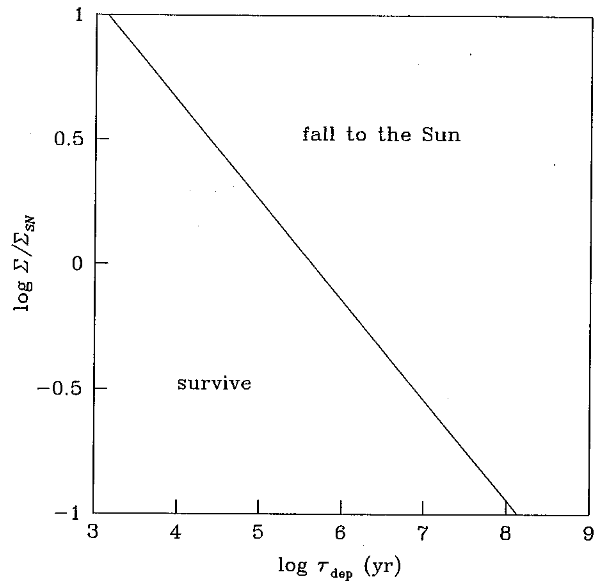

Figure 1.1: The disk surface density at 1AU as a function of gas depletion time scale obtained by equating $\tau_{\rm grav,mig}$ (eq.(2.12)) and $\tau_{\rm dep}$. Isolation mass $m_{\rm iso}$ is substituted for the mass.

time scale $\tau_{\rm dep}$. For $m_{\rm p}$ in eq.(2.12), the isolation mass, given by

$$m_{\rm iso} = 0.093 \left(\frac{\Sigma_{\rm s}}{\Sigma_{\rm s,SN}}\right)^{3/2} \left(\frac{a}{1{\rm AU}}\right)^{3/4} M_\oplus \tag{1.2}$$

(Kokubo and Ida 2002) is used. Planets can survive if the disk has surface density below the solid line for a given depletion time scale. The observationally inferred value for the depletion time scale is $\sim 10^6 - 10^7$ years (e.g., Haisch et al. 2001). If $\tau_{\rm dep} = 10^6$ years, the isolated protoplanets at 1 AU in MMSN can marginally survive. However, if $\tau_{\rm dep} = 10^7$ years, the protoplanets definitely fall to a host star. For safe survival, $\tau_{\rm dep} < 7 \times 10^5$ years is needed.

1.3 Migration Retardation Possibilities

One of the possibilities to alter the migration time scale in the terrestrial planet region is the inclusion of turbulance. which may be able to change the migration direction randomly (Laughlin et al. 2004, Nelson et al. 2004). However, it is unclear whether the total inward migration time scale is altered or not. Although the random component is added, there still exists the ordered monotonic inward migration component. The second possibility is the "type-II migration" (Lin and Papaloizou 1985, Ward 1997). Once a core exceeds a critical mass $\sim 10M_{\oplus}$, runaway gas accretion takes place (e.g. Mizuno 1980, Bodenheimer and Pollack 1986, Pollack et al. 1996) and forms a gap in a gas disk when the planet mass reaches $\gtrsim 10M_{\oplus}$ (Lin and Papaloizou 1985). The grown giant planet is trapped into the gap and migrate as the gap migrates toward the central star with a time scale that is $\sim 10^3$ times longer than the "type-I migration" time scale (Ward 1997). Ravikov (2002) studied the disk condition in terms of viscosity and disk aspect ratio for gap formation in a gas disk to find that a gap can form if the core's mass exceeds 2-15$M_{\oplus}$. Although the isolation mass (Kokubo and Ida 2002) at 5AU in MMSN is $\sim$ a few $M_{\oplus}$, which can marginally open up a gap, that in the terrestrial planet region ($\sim$ 1 AU) is $\sim 0.1M_{\oplus}$, which is too small for the gap formation. Hence, it is unlikely that type-I migration moves into type-II migration in the terrestrial planet region in MMSN.

1.4 Approach in this Paper

Another possibility for the change in the orbital migration is the gap formation in a planetesimal disk. The runaway protoplanets form gaps in the disk (Ward and Hahn 1995, Tanaka and Ida 1999). Ward and Hahn (1995) showed that a migrating protoplanet can shepherd the planetesimal disk by opening a gap if the migration is slow enough. Tanaka and Ida (1999) estimated the minimum migration time scale for the shepherding to take place. Gap formation leads to formation of a high density region inside the protoplanet's orbit, and it can slow down the inward migration speed. The migration retardation due to the shepherding of the planetesimal disk has not been examined in detail yet, and it may slow down the migration significantly.

Previous N-body simulations of planetesimal accretion have not included the type-I migration for simplification. In the present paper, we include both of the drag forces: the aerodynamical gas drag and the gravitational drag. We put one protoplanet seed in a planetesimal disk. The seed migrating inward can open a gap in planetesimal disk (Ida and Makino 1993, Tanaka and Ida 1997, 1999). We investigated how this gap affects the accretion and migration of the protoplanet and how long such retardation lasts. We included mutual gravitational interactions and coagulation of the planetesimals as well as the protoplanet-planetesimal interactions and accretion of the protoplanet. The torque from the disk gas that causes type-I migration is given as a parameter. We will show that the gap slows the migration. However, such period is short compared to the total migration time scale. The gap is eventually broken by the enhanced gravitational perturbation due to the growth of the planetesimals. We will also show that the accretion rate of the migrating protoplanet seed is not as fast as expected in the case without the gravitational interactions between the planetesimals in Tanaka and Ida (1999). As the planetesimals grow, their inclination increases and the growth rate can not be enhanced as predicted by them.

The migration and the formation process carries on with the existence of multiple protoplanets. Also, the disk gas dissipates with time. The protoplanets and planetesimals supplied from the outer region may affect the migration and accretion. In this paper, we also carry out N-body simulations with a wider disk including all these effects to see if the migration can be affected by them. We consider the growth of the planetesimals as well, by starting the simulations from the planetesimals. Ten simulations were performed, including the aerodynamical gas drag and the disk-planet interaction. We set the gravitational force become smaller exponentially with time. This treatment corresponds to the exponential depletion of the disk gas.

Initially heavy disk produces large protoplanets which migrate fast toward the central star. The accretion and the migration proceed from the inner region of the disk. As time evolves, the region that these processes take place moves to outer region. Meanwhile, the gas dissipates and the migration time scale for the protoplanets becomes longer. We check the migration and accretion of the runaway protoplanets and show that they are not affected by other protoplanets and planetesimals reside inner and outer orbits. We derived the analytical formula for time evolution of disk surface density as a function of the disk gas depletion time scale, which agrees well with N-body simulation results. The formula is based on the assumption that a protoplanet residing in a gas disk alone. The consistency between the analytical formula and the N-body results also shows that although a wider range of a disk with growth and multiple protoplanets are considered, the migration of a body proceeds as if it is placed in a gas disk alone.

The migration time scale has some uncertainty. If turbulence is considered, the migration time scale can be modified from the one that is derived assuming one protoplanet being in a gas disk. We introduce a migration retardation factor, which is a function of some constant and a initial gas to dust ratio of the planetesimal disk. By carrying out such treatment, we set constraints on the migration time scale for protoplanets to survive in disks with various gas to dust ratio. The difference between the remaining protoplanet disk after the gas depletion that included type-I migration and the model without the migration is discussed as well.

In the next chapter, the gap opening in the planetesimal disk is discussed, and in the third chapter, the effect of multiple protoplanets considering a wider disk is explained. Each chapter is divided into sections for simulation model explanation, the results and the summary. The chapters for the discussion and conclusion follows.

Chapter 2

Gap Formation in Planetesimal Disk

2.1 Model

2.1.1 Drag Forces

Aerodynamical Gas Drag

The aerodynamical gas drag force per unit mass takes is (Adachi et al. 1976)

$$\boldsymbol{f}_{\rm gas} = -\frac{1}{2m} C_{\rm D} \pi D \rho_{\rm gas} |\boldsymbol{u}| \boldsymbol{u}, \tag{2.1}$$

where $C_{\rm D} = 0.5$ is the gas drag coefficient, D is the body's physical radius and m is the mass. The disk gas density $\rho_{\rm gas}$ is written as

$$\rho_{\rm gas} = 1.4 \times 10^{-9} \left(\frac{\Sigma_{\rm g}}{\Sigma_{\rm g,SN}}\right) \left(\frac{r_{\rm p}}{1{\rm AU}}\right)^{-11/4} \quad ({\rm g\ cm^{-3}}), \tag{2.2}$$

where $r_{\rm p}$ is the body's distance from the central star. In eq(2.1) $\boldsymbol{u}$ is the relative velocity of the body and the disk gas, which is resulted in by orbital eccentriicity e and inclination i of the body and the deceleration of the disk gas velocity $v_{\rm gas}$ from the Kepler velocity $v_{\rm kep}$ due to pressure gradient given by Adachi et al. (1976)

$$\eta = \frac{v_{\rm kep} - v_{\rm gas}}{v_{\rm kep}} = 0.0019 \left(\frac{r_{\rm p}}{1{\rm AU}}\right)^{1/2} \tag{2.3}$$

where we used the temperature distribution of an optically thin disk (Hayashi 1981),

$$T_{\rm H} = 2.8 \times 10^{2} \left(\frac{r_{\rm p}}{1{\rm AU}}\right)^{-1/2} \quad ({\rm K}). \tag{2.4}$$

The gas drag causes damping of e and i and inward orbital migration. The time scale for e damping due to the gas drag is given with $\boldsymbol{u} \sim e v_{\mathrm{kep}}$ by

$$\tau_{\mathrm{gas}} = \frac{|\boldsymbol{u}|}{|\boldsymbol{f}_{\mathrm{gas}}|} \simeq 10^6 \left(\frac{m}{M_\oplus}\right)^{1/3} \left(\frac{\rho_{\mathrm{p}}}{3\mathrm{g\ cm^{-3}}}\right)^{2/3} \left(\frac{\Sigma_{\mathrm{g}}}{\Sigma_{\mathrm{g,SN}}}\right)^{-1} \left(\frac{r_{\mathrm{p}}}{1\mathrm{AU}}\right)^{13/4} \left(\frac{e}{0.01}\right)^{-1} \mathrm{years}. \tag{2.5}$$

Gravitational Drag due to Disk-Planet Interaction

A planet gravitationally perturbs the disk gas and excite density waves. It damps the planet's semimajor axis (Goldreich and Tremaine 1979,1980, Ward 1986, Korycansly and Pollack 1993, Tanaka et al. 2002) and eccentricity and inclination (Shu et al. 1983, Ward 1988, 1993, Artymowics 1993, 1994, Ward and Hahn 1994). Tanaka et al. (2002) and Tanaka and Ward (2004) carried out linear calculation to investigate three-dimensional density waves excited by a planet with mass m_{p}, eccentricity e_{p}, inclination i_{p} and semi-major axis a_{p}. They derive the forces exerted on the planet as follows.

$$f_{\mathrm{grav,r}} = \left(\frac{m_{\mathrm{p}}}{M_\oplus}\right)\left(\frac{a_{\mathrm{p}}\Omega_{\mathrm{p}}}{c}\right)^4 \Sigma_{\mathrm{g}} a_{\mathrm{p}}^2 \Omega_{\mathrm{p}} \left(2A_{\mathrm{r}}^{\mathrm{c}}\left[v_\theta - r_{\mathrm{p}}\Omega_{\mathrm{K}}(r_{\mathrm{p}})\right] + A_{\mathrm{r}}^{\mathrm{s}} v_{\mathrm{r}}\right). \tag{2.6}$$

$$\begin{aligned} f_{\mathrm{grav},\theta} &= \left(\frac{m_{\mathrm{p}}}{M_\oplus}\right)\left(\frac{a_{\mathrm{p}}\Omega_{\mathrm{p}}}{c}\right)^4 \Sigma_{\mathrm{g}} a_{\mathrm{p}}^2 \Omega_{\mathrm{p}} \left(2A_\theta^{\mathrm{c}}\left[v_\theta - r_{\mathrm{p}}\Omega_{\mathrm{K}}(r_{\mathrm{p}})\right] + A_\theta^{\mathrm{s}} v_{\mathrm{r}}\right) \\ &\quad +2.17\left(\frac{m_{\mathrm{p}}}{M_\oplus}\right)\left(\frac{a_{\mathrm{p}}\Omega_{\mathrm{p}}}{c}\right)^2 \Sigma_{\mathrm{g}} a_{\mathrm{p}}^3 \Omega_{\mathrm{p}}^2. \end{aligned} \tag{2.7}$$

$$f_{\mathrm{grav,z}} = \left(\frac{m_{\mathrm{p}}}{M_\oplus}\right)\left(\frac{a_{\mathrm{p}}\Omega_{\mathrm{p}}}{c}\right)^4 \Sigma_{\mathrm{g}} a_{\mathrm{p}}^2 \Omega_{\mathrm{p}} \left(2A_{\mathrm{z}}^{\mathrm{c}} v_{\mathrm{z}} + A_{\mathrm{z}}^{\mathrm{s}} z \Omega_{\mathrm{p}}\right). \tag{2.8}$$

where c is the sound speed, Ω_{p} is the Keplerian angular velocity at a_{p} and v_θ, v_{r} are azimuthal and radial velocities of the planet respectively. The second term of $f_{\mathrm{grav},\theta}$ damps a_{p}. The other terms in $f_{\mathrm{grav,r}}$ and $f_{\mathrm{grav},\theta}$ damp e_{p} and $f_{\mathrm{grav,z}}$ damps i_{p}. The coefficients are

$$A_{\mathrm{r}}^{\mathrm{c}} = 0.057, \qquad A_{\mathrm{r}}^{\mathrm{s}} = 0.176, \tag{2.9}$$

$$A_\theta^{\mathrm{c}} = -0.868, \qquad A_\theta^{\mathrm{s}} = 0.325, \tag{2.10}$$

$$A_{\mathrm{z}}^{\mathrm{c}} = -1.088, \qquad A_{\mathrm{z}}^{\mathrm{s}} = -0.871. \tag{2.11}$$

In MMSN, the migration time scale is

$$\tau_{\mathrm{grav,mig}} = 7.0 \times 10^4 \left(\frac{m_{\mathrm{p}}}{M_{\oplus}}\right)^{-1} \left(\frac{r_{\mathrm{p}}}{1\mathrm{AU}}\right)^{3/2} \left(\frac{\Sigma_{\mathrm{g}}}{\Sigma_{\mathrm{g,SN}}}\right)^{-1} \text{years} \tag{2.12}$$

The damping time scales of eccentricity and inclination are

$$\tau_{\mathrm{grav,e}} = 1.3\tau_{\mathrm{grav}}, \quad \tau_{\mathrm{grav,i}} = 1.8\tau_{\mathrm{grav}} \tag{2.13}$$

where

$$\tau_{\mathrm{grav}} = \left(\frac{m_{\mathrm{p}}}{M_{\odot}}\right)^{-1} \left(\frac{\Sigma_{\mathrm{g}} a^2}{M_{\odot}}\right)^{-1} \left(\frac{c}{a\Omega_{\mathrm{p}}}\right)^4 \Omega_{\mathrm{p}}^{-1} = 4 \times 10^2 \left(\frac{r_{\mathrm{p}}}{1\mathrm{AU}}\right)^2 \left(\frac{m_{\mathrm{p}}}{M_{\oplus}}\right)^{-1} \left(\frac{\Sigma_{\mathrm{g}}}{\Sigma_{\mathrm{g,SN}}}\right)^{-1} \text{years} \tag{2.14}$$

Comparison of Eqs.(2.5) and (2.14) shows that the disk-planet interaction becomes dominant over aerodynamical gas drag for $m_{\mathrm{p}} \gtrsim 0.003 M_{\oplus}$, if $e \sim 0.01$.

2.1.2 Method of Calculation

Initial Distribution of a Protoplanet and Planetesimals

We carried out 6 simulations, RunB0.5, RunB1, RunB2, RunB3, RunB4 and RunB5. The number "x" in RunB"x" represents the value of an enhancement factor B_{grav} defined below. Each of them starts with 8410 planetesimals, ranging from 0.9 AU to 1.1 AU, and one runaway protoplanet seed is placed at 1.05AU. Protoplanet's mass is 3×10^{26} g and each planetesimal has a mass of 3×10^{23} g. The radial distribution of the planetesimals follows $\Sigma_{\mathrm{s,SN}}$. It is suggested that runaway growth starts when the planetesimal mass is as small as $\sim 10^{19} - 10^{20}$ g (Ohtsuki et al 1993, Inaba et al. 2001). Our adopted value of the planetesimal mass is set to be much larger than it should be to save the simulation time. In order to reproduce the same strength of drag force on smaller planetesimals, the aerodynamical gas drag for planetesimals is enhanced by a factor of 40 from that in MMSN. This enhanced drag force on a 3×10^{23}g body corresponds to the normal drag force on a 5×10^{18}g body in MMSN. The strong drag force on planetesimals tends to facilitate the gap formation by a protoplanet (Tanaka and Ida 1999).

Scaling of a Migration Parameter

Although we adopt $\Sigma_{\rm s,SN}$, gas and solid components can move independently, so that $\Sigma_{\rm g}$ can differ from $\Sigma_{\rm g,SN}$. To take into account such an effect (and for other possible effects to change the numerical factors $\boldsymbol{f}_{\rm grav}$), we introduce an enhancement parameter $B_{\rm grav}$, such as $\boldsymbol{f}_{\rm grav} = B_{\rm grav}\boldsymbol{f}_{\rm grav,SN}$, where $\boldsymbol{f}_{\rm grav,SN}$ is $\boldsymbol{f}_{\rm grav}$ with $\Sigma_{\rm g} = \Sigma_{\rm g,SN}$. The value of $B_{\rm grav}$ in each simulation is listed in Table I.

A protoplanet pushes away the planetesimals through gravitational scattering with the help of self-gravity of planetesimals (Ida and Makino 1993) and gas drag (Tanaka and Ida 1996) and forms a gap in a planetesimal swarm. As the protoplanet migrates inward, planetesimals inside the orbit of the protoplanet tend to approach the protoplanet. The gravity of the protoplanet tends to push them away while the recoil pushes back the protoplanet. This process is called "shepherding" of planetesimals by a protoplanet (Ward and Hahn 1995). If shepherding occurs, torque exerted on a protoplanet by a gas disk is transported into the planeteimal disk, so that the migration of the protoplanet slows down.

However, shepherding does not always take place. For fast migration, it is difficult for the shepherding to take place. Tanaka and Ida (1999) estimated a critical migration time scale $\tau_{\rm mig,crit}$ for shepherding to occur (e.g. fig.5 of Tanaka and Ida 1999). The protoplanet can shepherd the planetesimals if $\tau_{\rm grav,mig} > \tau_{\rm mig,crit}$. For a protoplanet with mass of 3×10^{26} g and the aerodynamical gas drag being enhanced by the factor of 40,

$$\tau_{\rm mig,crit} = 3.1 \times 10^5 T_{\rm K}, \tag{2.15}$$

where $T_{\rm K}$ is the Keplerian period. Equation (2.12) with $m_{\rm p} = 3 \times 10^{26}$ g reads as

$$\tau_{\rm grav,mig} = 1.4 \times 10^6 B_{\rm grav}^{-1} T_{\rm K}. \tag{2.16}$$

Hence, Shepherding should take place in the simulations with

$$B_{\rm grav} \lesssim B_{\rm grav,crit} = 4, \tag{2.17}$$

according to their estimation. However, Tanaka and Ida (1999) did not take into account the gravitational interactions between the planetesimals and their growth. These effects are included in our simulations. We will show that these effects inhibit shepherding.

2.1.3 N-body Simulation Scheme

We integrate orbits with 4th order Hermite scheme (Makino and Aarseth 1992) with hierarchical individual time step (Makino 1991). The equation of motion is written as below.

$$\frac{\mathrm{d}\boldsymbol{v}_j}{\mathrm{d}t} = -\frac{GM_\odot}{|\boldsymbol{r}_j|^3}\boldsymbol{r}_j - \sum_{j \neq k} \frac{GM_j}{|\boldsymbol{r}_j - \boldsymbol{r}_k|^3}(\boldsymbol{r}_j - \boldsymbol{r}_k) + \boldsymbol{f}_{\mathrm{gas}} + \boldsymbol{f}_{\mathrm{grav}} \tag{2.18}$$

where $\boldsymbol{r}_j$ is the heliocentric position vector of particle j. The first term is gravity of the central star, the second term is mutual gravity between the particles, the third term $\boldsymbol{f}_{\mathrm{gas}}$ is aerodynamical gas drag and the last term $\boldsymbol{f}_{\mathrm{grav}}$ is drag due to tidal interaction with a gas disk, as explained in section 2.1. Since the total mass of the planetesimals (and the protoplanets) is $\sim 10^{-6}$ times the mass of the central star, we neglect the indirect term.

When the distance between two bodies becomes less than the sum of their radii, we consider the bodies to merge, assuming perfect accretion. Physical radius of a body is determined by its mass m_{p} and internal density ρ_{p} as

$$D = \left(\frac{3}{4\pi}\frac{m_{\mathrm{p}}}{\rho_{\mathrm{p}}}\right)^{1/3}. \tag{2.19}$$

We adopt 3g cm^{-3} as ρ_{p}. In order to shorten the calculation time, we enhance the collisions by expanding the physical radii of the bodies by 5 times as in Kokubo and Ida (1996).

2.2 Results

2.2.1 Short Term Orbital Evolution

The time scale of gravitational stirring of planetesimal eccentricities $\langle\tilde{e}^2\rangle^{1/2}$ due to perturbations from a protoplanet with $m_{\rm p}$ is (Ida and Makino 1993)

$$\tau_{\rm VS} \sim 1\times 10^3 \left(\frac{a}{1{\rm AU}}\right)^{3/2} \left(\frac{\langle\tilde{e}^2\rangle^{1/2}}{2}\right)^4 \left(\frac{m_{\rm p}}{3\times 10^{26}{\rm g}}\right)^{1/3} \text{ (years)}. \tag{2.20}$$

The eccentricities and inclinations are normalized with $h_{\rm p}$ as below.

$$\tilde{e} = \frac{e}{h_{\rm p}}, \quad \tilde{i} = \frac{i}{h_{\rm p}} \tag{2.21}$$

where

$$h_{\rm p} = \left(\frac{m_{\rm p}}{3M_\odot}\right)^{1/3}. \tag{2.22}$$

A gap will be opened up in the planetesimal disk on this time scale, if diffusion of the planetesimal swarm and migration of the protoplanet do not exist. As described in the previous section, the analytical estimate by Tanaka and Ida (1999) suggests that a gap formation is inhibited by the migraiton if $B_{\rm grav} \gtrsim B_{\rm grav,crit} = 4$.

To see the migration effects, we plot the snapshots on $\tilde{e}$-a plane at $t = 5000$ years of each simulation in Fig.2.1. Since $\langle\tilde{e}^2\rangle^{1/2} \sim 2$ and $m_{\rm p} \sim 3\times 10^{26}$g in our calculations, $\tau_{\rm VS}$ is sufficiently shorter than 5000 years. In the snapshots, two thick lines in each of the snapshots are $E_{\rm J} = 0$ lines, where Jacobi energy $E_{\rm J}$ is defined by (Hayashi et al. 1977)

$$E_{\rm J} = \frac{1}{2}\left(\tilde{e}^2 + \tilde{i}^2\right) - \frac{3}{8}\tilde{b}^2 + \frac{9}{2} \tag{2.23}$$

and

$$\tilde{b} = \frac{a - a_{\rm p}}{h_{\rm p} a_{\rm p}}. \tag{2.24}$$

We used $\tilde{e} \sim 0$ and $\tilde{i} \sim 0$ to draw the $E_{\rm J} = 0$ lines. Only planetesimals in $E_{\rm J} > 0$ region between the two lines can closely approach the protoplanet. RunB0.5, RunB1, RunB2 and RunB3 show "clear gap" formation, where a clear gap means that few planetesimals exist in the $E_{\rm J} > 0$ region. In RunB4, small amount of planetesimals are left in the

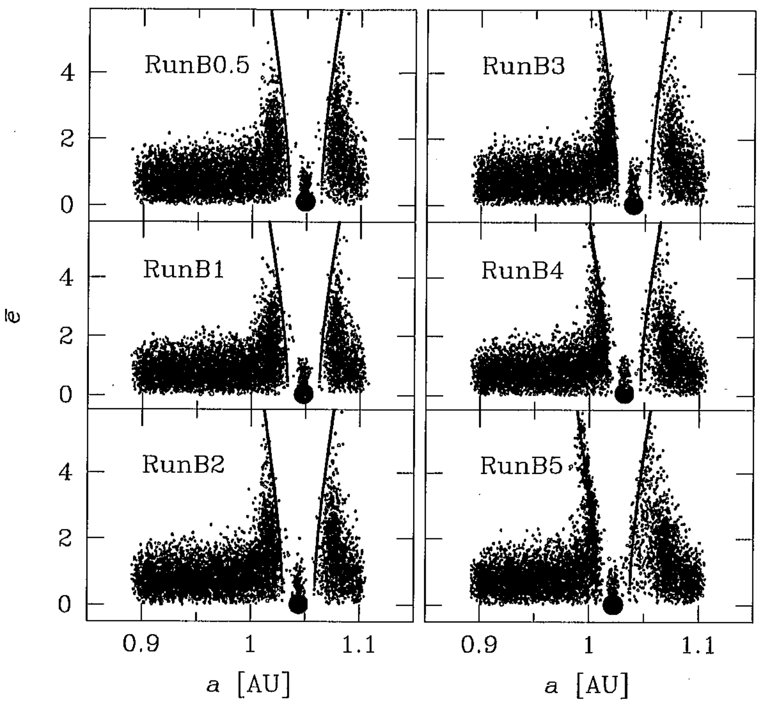

Figure 2.1: Snapshots on $\tilde{e}$-a plane of all the simulations at $t = 5000$ years. Size of the dots are proportional to the radius of the particles. Particles with $m > 2 \times 10^{25}$g are in solid circles. Two solid lines are $E_J = 0$ lines. Significant amount of planetesimals are in the $E_J > 0$ region in RunB4 and RunB5.

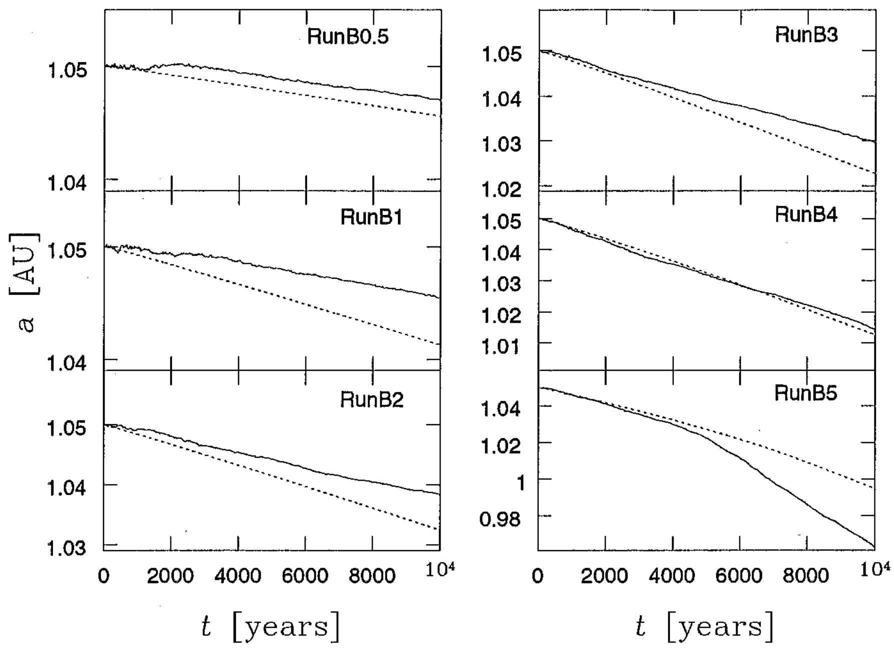

Figure 2.2: Time evolution of the semimajor axis of the proplanet seed of every simulation during the first 10^4 years. The dotted lines are the analytical estimates derived by using $\tau_{\rm grav,mig}$. The solid lines are the N-body simulation results.

$E_{\rm J} > 0$ region, indicating the gap opening is marginal. Clear gap formation is apparently inhibited in RunB5. These results are consistent with the analytical condition of gap formation, $B_{\rm grav} < B_{\rm grav,crit} \simeq 4$.

The semimajor axis evolution of the protoplanet seed during the first 10^4 years is shown in Figure 2.2. The dotted lines are the analytical solution derived by $\tau_{\rm grav,mig} = a_{\rm p}({\rm d}a_{\rm p}/{\rm d}t)^{-1}$ with eq.(2.16). They show the evolution without any migration retardation. The solid lines are the simulation results. In RunB0.5 - 3, as the gaps are formed, the gradient of the solid lines becomes smaller than the analytical lines. The migration is retarded by the shepherding due to a gap formation in the planetesimal disk. In RunB4, the solid line and the dotted line are almost the same. Since a gap in the planetesimal disk is not clear enough, the migration retardation can not take place. RunB5 resulted in even faster migration than the analytical speed. The close encounters with planetesimals in $E_J > 0$ also induce inward migration of the seed in addition to the inward migration due to the gravitational drag, as explained later, resulting in faster migration than the analytical estimation.

In our simulations, when $B_{\rm grav} < 4$, clear gap formation and migration retardation are apparent. When $B_{\rm grav} \geq 4$, a gap can be opened, however, the migration is not retarded (rather accelerated in the $B_{\rm grav} = 5$ case). Hence, in the short term, the N-body simulation results are consistent with the analytical estimate.

2.2.2 Long Term Evolution

Orbital Evolution

Although a gap opening and the migration retardation are apparent in the short term ($\lesssim 10^4$ years) in RunB0.5-3, they are not maintained in a longer term. Figure 2.3 is the semimajor axis evolution of the protoplanet seed in each case. The migration retardation ceases after $t = 3.5 \times 10^4, 3 \times 10^4, 2.5 \times 10^4$ and 2.0×10^4 years in RunB0.5, RunB1, RunB2 and RunB3, respectively. Figure 2.4 shows the $\tilde{e}$-a plane snapshots in each case, after the gap is broken. Planetesimals start to fill $E_J > 0$ region from small a region. They undergo close encounters with the protoplanet seed and are thrown behind the seed. As a result, the seed loses angular momentum, gaining more inward migration (Ida et al. 2000, Gomes et al. 2004). When the transport of the planetesimals starts, a large amount of planetesimal is thrown behind at once as an avalanche, since a high density region has been formed in front of the protoplanet seed. The avalanche results in a sudden increase in the migration speed of the seed, as in Figure 2.3. It becomes even faster than the analytical value, temporarily. After the avalanche event, the migration speed becomes almost the same as the analytical value. Although the acceleration of the migration should keep going as close encounters with inner planetesimals are more dominant than

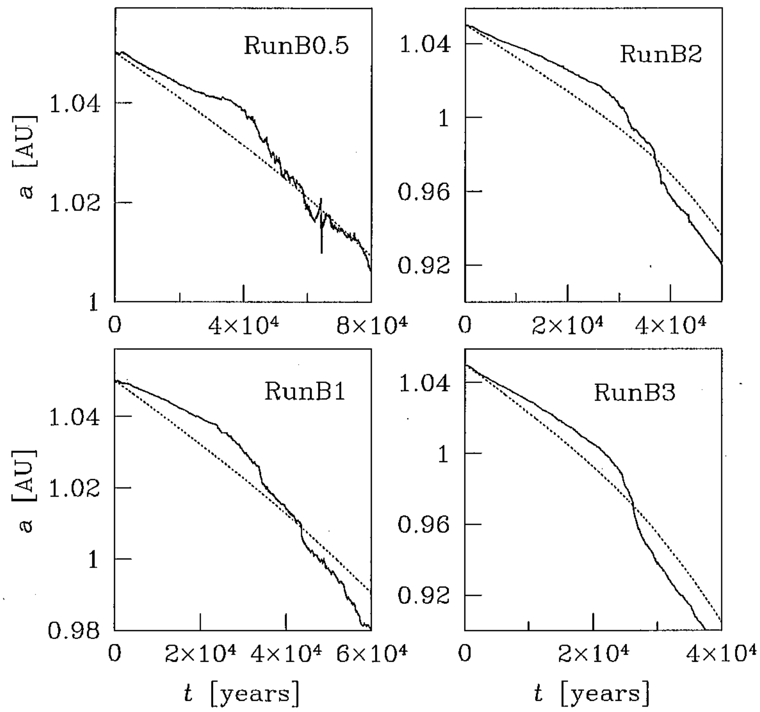

Figure 2.3: Time evolution of the semimajor axis of the proplanet seed of RunB0.5, RunB1, RunB2 and RunB3 for longer period than 10^4 years. The notations are the same as in Fig.2.3.

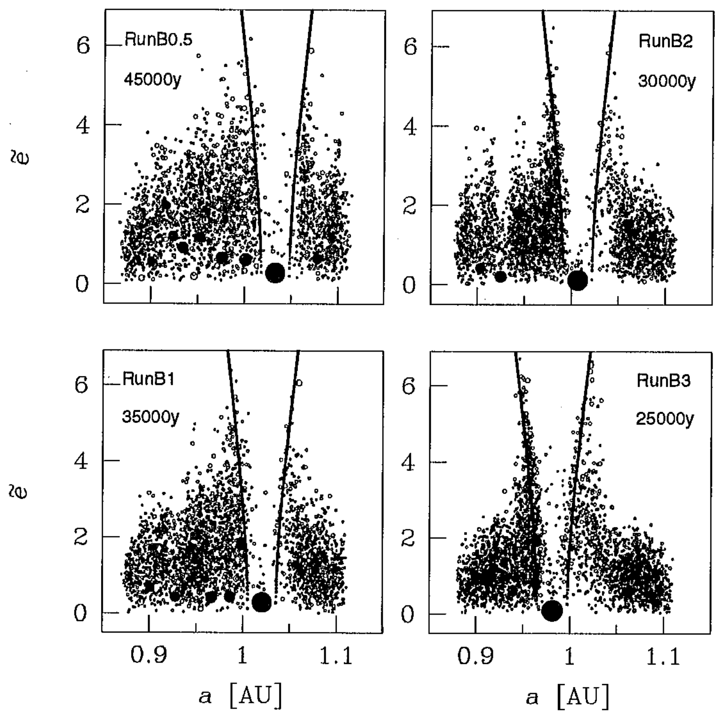

Figure 2.4: Snapshots of $\tilde{e}$-a plane of RunB0.5 at $t = 4.5\times10^4$ years, RunB1 at $t = 3.5\times10^4$ years, RunB2 at $t = 3.0 \times 10^4$ years, and RunB3 at $t = 2.5 \times 10^4$ years. The notation is the same as in Fig.2.1

those with outer ones (Ida et al. 2000, Gomes et. al. 2004), it is not apparent. In RunB5, such avalanche starts in the early stage of the simulation. Although the gap is not clear, amount of planetesimal that resides right inside the protoplanet's orbit is large, which causes the early avalanche event.

The Break Down of Gaps

The time when the retardation stops has $B_{\rm grav}$ dependency. Table II is the list of the time scales and the masses of the planetesimals at the gap break down.

The larger $B_{\rm grav}$ is, the shorter the gap break-down time ($T_{\rm break}$) the simulation has. As discussed below, the slower the migration is, the larger planetesimal mass ($m_{\rm break}$) is needed to break the gap. The growth time scale $T_{\rm grow}$ of a body with mass $m_{\rm break}$ is (Kokubo and Ida 2002)

$$\begin{aligned} T_{\rm grow} &= m_{\rm break}/\dot{m}_{\rm break} \quad (2.25)\\ &= 7.8\times 10^3 \langle \tilde{e}^2 \rangle \left(\frac{C}{2}\right)^2 \left(\frac{m_{\rm break}}{10^{26}{\rm g}}\right)^{1/3} \left(\frac{\rho_{\rm p}}{3{\rm g\,cm^{-3}}}\right)^{1/3} \\ &\quad \left(\frac{\Sigma_{\rm solid}}{7{\rm g\,cm^{-2}}}\right)^{-1} \left(\frac{a}{1{\rm AU}}\right)^{1/2} ({\rm years}). \quad (2.26) \end{aligned}$$

Since $T_{\rm grow}$ increases with $m_{\rm break}$, and $m_{\rm break}$ for the gap break down decreases with $B_{\rm grav}$, the dependence of $T_{\rm break}$ on $B_{\rm grav}$ can be accounted for by $T_{\rm grow}$.

The dependence of $m_{\rm break}$ on $B_{\rm grav}$ is explained as follows. The planetesimals placed close to $E_{\rm J} = 0$ region begin to grow when the gap is made. When the planetesimals grow, the gravitational interactions between the planetesimals become stronger. Such interaction causes the planetesimals to move into $E_{\rm J} > 0$ region, where they can interact with the protoplanet seed. The seed loses the angular momentum as it throws the planetesimals behind, and gains the migration speed. Once this reaction starts, a large amount of planetesimals that resided around $E_{\rm J} = 0$ is translated to the outer orbit of the seed at once, and the avalanche migration of the seed takes place.

When the migration speed is 0, $m_{\rm pl,max}$ for the gap to be filled can be estimated by the condition for the dominance of protoplanet-planetesimal interactions relative to planetesimal-planetesimal interactions obtained by Ida and Makino (1993) as

$$\frac{m_{\mathrm{p}}}{m} < 30 \left(\frac{m}{10^{23}\mathrm{g}}\right)^{-2/5} \left(\frac{a}{1\mathrm{AU}}\right)^{3/10}, \tag{2.27}$$

if $\langle \tilde{e}^2 \rangle^{1/2} \sim 2$. When the protoplanet seed has a mass of $\sim 3 \times 10^{26}$g, $m_{\mathrm{pl,max}} = 2 \times 10^{26}$g. The growth time scale for such a mass is $\sim 2.3 \times 10^4$ years (Kokubo and Ida 2002). This time scale is the upper limit for the gap to break. As the migration becomes faster, $m_{\mathrm{pl,max}}$ for breaking the gap becomes smaller. Hence, T_{break} ($\sim T_{\mathrm{grow}}$) needed for gap disappearance is shorter.

The Case with Smaller Initial Mass of Planetesimals

From the analytical estimate, a clear gap opening and shepherding occur if the migration speed satisfies $B_{\mathrm{grav}} < 4$. Our simulations show the results consistent with the analytical estimate in short term, but the shepherding only lasts for the growth time scale to $m_{\mathrm{pl,max}}$. Our simulations start with relatively large planetesimals for computational reason. A realistic initial mass of planetesimals may be much smaller. However, even if the initial mass is 10^{20}g and radius enhancement factor $f = 1$, $T_{\mathrm{grow}}(T_{\mathrm{break}}) < 2 \times 10^5$ years, which is shorter than the gas disk life time ($\sim 10^6$-10^7 years). Hence, even if realistic initial mass of planetesimals is considered, our conclusion that the shepherding can not last long enough, and that the gap formation in a planetesimal disk can not retard type-I migraiton does not change.

2.2.3 Growth of the Protoplanet

The growth of the protoplanet seed is affected by the evolution of planetesimal disk as well. Figure 2.5 shows the mass evolution of the protoplanet seed of RunB5, RunB4, RunB3, and RunB2. The dotted line is the analytical estimate that is derived by Tanaka and Ida (1999) as

$$\frac{\mathrm{d}M_{\mathrm{p}}}{\mathrm{d}t} = 2\pi h_{\mathrm{p}}^2 a_{\mathrm{p}}^2 \Sigma_{\mathrm{solid}} < P_{\mathrm{col}} > T_{\mathrm{K}}^{-1}. \tag{2.28}$$

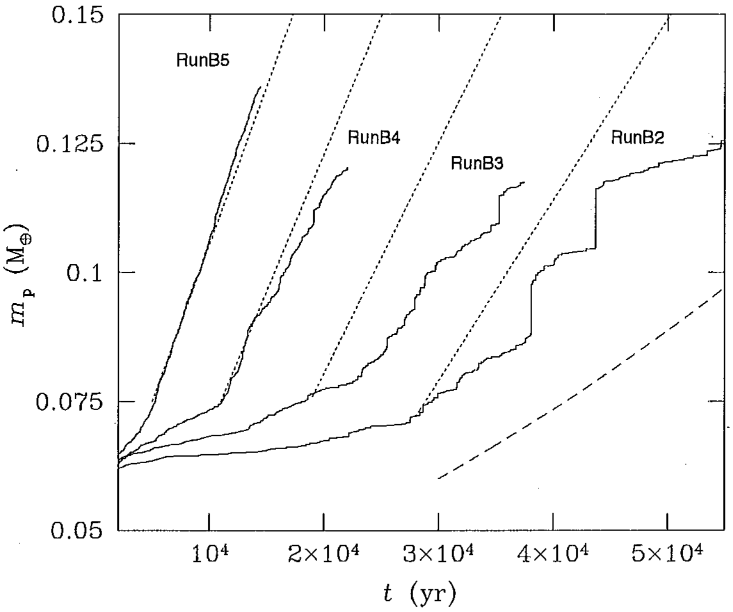

Figure 2.5: Time evolution of the mass of protoplanet seed in RunB5, RunB4 RunB3 and RunB2. The dotted line is the analytical estimate that is derived by Tanaka and Ida (1999). The collistion rate is multiplied by 2 because of the enhancement due to the gas drag. Solid lines are the N-body simulation results. The dashed line is drawn assuming no migration.

Considering the aerodynamical gas drag effect, the collision rate (eq.(3.20) in Tanaka and Ida,1999) becomes larger by factor of ~ 2. For the inclination, the escape velocity of the initial planetesimals is used ($\tilde{i}_{0,\rm esc} = 0.76$). The results of RunB5 and RunB4 agree well with the analytical estimate. However, as the migration becomes slower, the rate becomes smaller in the N-body simulation results than the analytical estimate, as in RunB3 and RunB2. This is due to the increase of the planetesimals' inclination. The larger inclination makes the growth rate become smaller (Tanaka and Ida 1999). The average inclination of the planetesimals is $\langle \tilde{i}^2 \rangle^{1/2} \sim 0.82$ at $t = 3 \times 10^4$ years in RunB3, and $\langle \tilde{i}^2 \rangle^{1/2} \sim 1.22$ at $t = 4 \times 10^4$ years in RunB2. These values are larger than $\tilde{i}_{0,\rm esc} = 0.76$. This inclination increase is due to the growth of the planetesimals. The planetesimals have longer time to grow in the slower migration cases. As the planetesimals grow, their escape velocity becomes larger as well. The growth of the planetesimals lowers the growth rate of the protoplanet seed. However, although there is a difference in the rate as the planetesimals grow, the difference is factor of ~ 2 in RunB2 and RunB3.

As mentioned earlier, our simulations start with rather large planetesimals for computational reason. If we consider smaller planetesimals, the inclination of the planetesimals will be smaller and the growth rate becomes as large as that estimated in Tanaka and Ida (1999), which is about ten times larger than the case with no migration (Kokubo and Ida 2002). However, such small planetesimals grow quickly. The dashed line in Fig 2.5 is drawn assuming no migration. The growth rate of RunB5 is ~ 3 times that of the case with no migration. Planetesimals with intial mass of 10^{20}g will grow to the size of 10^{23} g in $\sim 10^4$ years (Kokubo and Ida 2002). As they grow, the inclination becomes higher. Hence, high growth rate period will not last and quickly decreases to ~ 3 times the case of no migration (dashed line). Such a high growth rate period does not sustain long even if we consider the smaller initial planetesimals because of the growth of the protoplanets.

2.3 Summary

The speed of type-I migration can be altered if the torque exerted by the planetesimal disk is considered. If a gap is formed in the planetesimal disk around the protoplanet's orbit, the radial motions of the disk and the protoplanet are coupled through shepherding. Then, in order for the protoplanet to be pushed inward by tidal interaction with a gas disk, angular momentum of the protoplanet and the planetesimal disk as a whole needs to be removed. As a result, the migration of the protoplanet can be retarded if the mass of the planetesimal disk is larger than that of the protoplanet. We have performed N-body simulations on formation of protoplanets including aerodynamical gas drag and drag force due to disk-planet interaction. The simulations were done with one protoplanet seed embedded in a planetesimal disk in order to study the effect of planetesimal disk torque exerted on the migrating protoplanet. Six simulations were performed, with variation of the migration speed; the speed that is equivalent with $B_{\rm grav}$ times that in MMSN ($B_{\rm grav}$ =0.5, 1, 2, 3, 4 and 5). The main results are in the following.

1. During the first $\sim 10^4$ years, clear gap formation and shepherding take place in the simulations with $B_{\rm grav} < B_{\rm grav,crit} = 4$, as the analytical estimate predicted.

2. However, the gap is not sustained for more than 10^5 years. The time scale for the gap to break down ($T_{\rm break}$) is shorter for faster migration, and is related to the planetesimal growth time scale. A clear gap breaks when the gravitational interactions between the planetesimals become strong enough to push each other inside $E_{\rm J} > 0$ region. Such a planetesimal mass for breaking the gap ($m_{\rm pl,max}$) is larger for slower migration. In reality, initial planetesimals are much smaller than we used in our simulations. However, the growth time scale for them to become $m_{\rm pl,max}$ is significantly shorter than the disk life time. Hence, the gap break-down mechanism is not affected largely by the initial planetesimal mass.

3. The accretion rate of the migrating protoplanet seed is not as fast as expected in the case without the gravitational interactions between the planetesimals in Tanaka and Ida

(1999). Initially, when the planetesimals are small ($\lesssim 10^{20}$ g), the growth rate would be ~ 10 times as the case with no migration as they say in Tanaka and Ida (1999). However, they quickly grow ($\sim 10^4$ years) and their gravitational interactions become stronger, increasing the inclinations among themselves. Such high inclinations lower the growth rate by half or more.

Inclusion of the torque from the planetesimal disk does not have significant effect on the type-I migration. So far, we have considered one protoplanet seed in a planetesimal disk in a limited range of semimajor axis. The planet formation proceeds with multiple protoplanets. The interaction between the protoplanets may alter the result. Large bodies that form in outer regions, migrating inward can also influence the growth of protoplanets in inner regions. We will investigate such effects in the following chapter.

2.4 Tables

Table I

Simulation Parameters of RunB0.5 - RunB5

Run	B_{grav}
RunB0.5	0.5
RunB1	1
RunB2	2
RunB3	3
RunB4	4
RunB5	5

For all of the runs, the planetesimal disk ranges from 0.9 - 1.1 AU. Protoplanet's mass $m_{\mathrm{p}} = 3 \times 10^{26}$g and each planetesimal's mass $m_{\mathrm{pla}} = 3 \times 10^{23}$g. The protoplanet is initially placed at 1.05 AU. Initial total number of bodies is 8410. The planetesimals are placed to fit the minimum mass disk model. The migration speed is measured by B_{grav}.

Table II

Migration Speed and the Gap Break-Down

B_{grav}	0	0.5	1	2	3
T_{break}(yr)	-	3.5×10^4	3×10^4	2.5×10^4	2×10^4
$m_{\mathrm{pl,max}}$(g)	1.8×10^{26}	8×10^{25}	2×10^{25}	1.4×10^{25}	8×10^{24}
T_{grow}(yr)	2.3×10^4	2.5×10^4	1.6×10^4	1×10^4	8×10^3

List of the gap break down time T_{break}, and the maximum planetesimal mass $m_{\mathrm{pl,max}}$ around the vicinity of the protoplanet seed (region with $a < a_{\mathrm{p}}$ and $-25 < E_{\mathrm{J}} < 0$) at T_{break}. For the growth time scale T_{grow}, we used eq(6) in Kokubo and Ida (2002) with the parameters in our simulation. For the eccentricity, the equillibrium eccentricity for 3×10^{23}g is used ($(\langle \tilde{e}_{\mathrm{eq}}^2 \rangle)^{1/2} \sim 3.5$). When $B_{\mathrm{grav}} = 0$, there is no migration. Analytical estimate from Ida and Makino (1993) is listed in the $B_{\mathrm{grav}} = 0$ column. When $B_{\mathrm{grav}} = 1, 0.5$, $\Sigma_{\mathrm{s}}/\Sigma_{\mathrm{s,SN}} \sim 0.7$ in the simulations at $t = T_{\mathrm{break}}$. We substituted $\Sigma_{\mathrm{s}}/\Sigma_{\mathrm{s,SN}} = 1$ for $B_{\mathrm{grav}} = 0$.

Chapter 3

Effect of Multiple Protoplanets and Other Planetesimals

3.1 Model

The model we incorporated in the second set of simulations are the same as in the previous set, except for the exponential weakening of the gravitational drag force, and the initial distribution of the planetesimals.

3.1.1 Initial Distribution of Planetesimals

We carried out 10 simulations, Run1-10. The initial conditions are listed in Table III. The parameters for the planetesimal distribution are the outer boundary $a_{\rm max}$ of the planetesimal disk, and the initial solid surface density $\Sigma_{\rm s,init}$. The mass of each planetesimal is $m_{\rm pla}$, and the initial number of planetesimals is N. It is suggested that the runaway growth starts when the planetesimal mass is 10^{19}-10^{20}g (Ohtsuki et al. 1993, Inaba et al. 2001). We adopted a planetesimal mass that is much larger than it should be in order to save the simulation time. In order to reproduce the same strength of drag force on smaller planetesimals, the aerodynamical gas drag for planetesimals is enhanced by factor of 40, as in previous set of simulations.

3.1.2 Migration Enhancement Parameter

As in the previous set of simulations, we incorporated $B_{\rm grav}$ for migration enhancement factor and adopt $\boldsymbol{f}_{\rm grav} = B_{\rm grav}\boldsymbol{f}_{\rm grav,SN}$, where $\boldsymbol{f}_{\rm grav,SN}$ is the gravitational drag with $\Sigma_{\rm g} = \Sigma_{\rm g,SN}$ at $t = 0$. The factor $B_{\rm grav}$ corresponds to the amount of gas. We assume the exponential decay of the gas disk,

$$\Sigma_{\rm g}(t) = \Sigma_{\rm g,0} \exp\left(-\frac{t}{\tau_{\rm dep}}\right) \tag{3.1}$$

where $\Sigma_{\rm g,0}$ is the initial gas surface density and $\tau_{\rm dep}$ is the gas depletion time scale. Correspondingly,

$$\boldsymbol{f}_{\rm grav}(t) = B_{\rm grav}\boldsymbol{f}_{\rm grav,SN} \exp\left(-\frac{t}{\tau_{\rm dep}}\right), \tag{3.2}$$

that is, the gravitational drag is parameterized by $B_{\rm grav}$ and $\tau_{\rm dep}$. The parameters in each of the simulations are listed in Table III. The initial solid surface density and the initial migration enhancement factor is the same, that is, the initial gas to dust ratio is set to be the same.

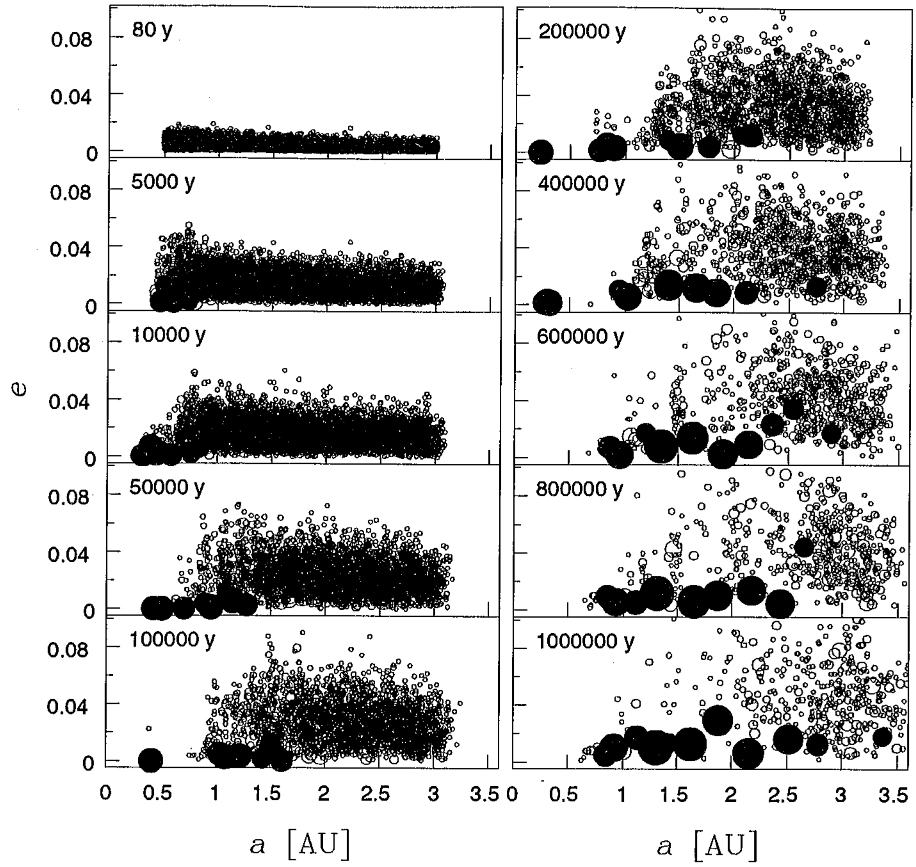

Figure 3.1: Orbital evolution of Run4 on e-a plane. The size of the dot is proportional to the radius of the body. The solid dots indicate the bodies with $m > 0.2M_{\oplus}$.

3.2 Results

3.2.1 Effects from the Inner Bodies

Figure 3.1 shows the mass and orbital evolution of Run4 ($\tau_{\rm dep} = 10^5$ years, $B_{\rm grav} = 5$). Since the accretion time scale is shorter in the inner region, runaway growth takes place in the inner region faster than in the outer region. The runaway bodies migrate to the central star as they grow. The accretion time scale of the inner runaway protoplanets are shorter than the ones in the outer region. Since the migration time scale is shorter with the larger mass and smaller semimajor axis, the migration time scale of the inner runaway bodies are considerably shorter than the outer ones. Figure 3.2 shows the migration time

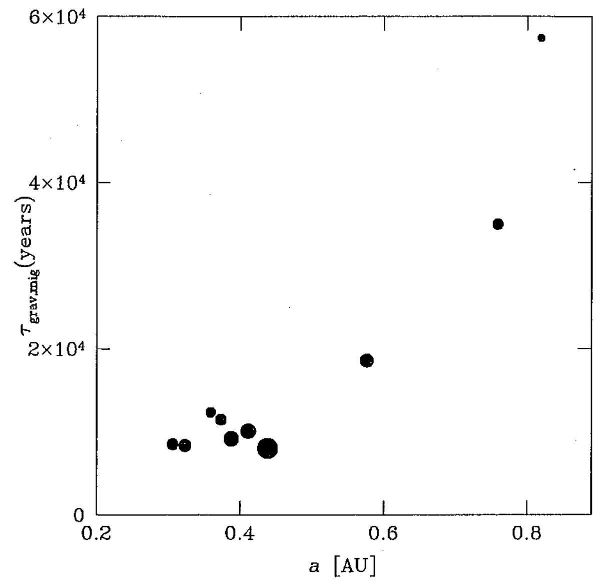

Figure 3.2: Migration time scale $\tau_{\rm grav,mig}$ and the a of runaway bodies with $m > 0.2M_\oplus$ at $t = 10^4$ years in Run4. The size of the dots is proportional to the mass of the protoplanet.

scale for the runaway protoplanets with $m > 0.2M_\oplus$ at $t = 10^4$ years. The size of the circle is proportional to the mass of the protoplanet. The ones at ~ 0.3 AU were formed at ~ 0.5AU and migrated during the first 10^4 years. This leads to faster solid material depletion in the inner region.

Figure 3.3 shows the semimajor axis evolution of the largest protoplanets that emerged at $t \sim 5000$ years and $t \sim 1.3 \times 10^4$ years. They fall toward the central star on time scales $\sim 10^4$ years. The dotted lines are the analytical solution derived by $\mathrm{d}a_\mathrm{p}/\mathrm{d}t = a_\mathrm{p}/\tau_\mathrm{dep}$ and eq.(2.12), which assumes one body being in a gas disk alone. The solid lines are the simulation results. The embryo that emerged at $t \sim 5000$ years has a mass of $\sim 0.5M_\oplus$, and the one emerged at $t \sim 1.3 \times 10^4$ years has $\sim 0.7M_\oplus$. The gradient of the solid lines are ~ 0.92 times that of the analytical line for the left one, and ~ 0.84 for the right one. The small retardation may be due to the perturbations from the other large bodies in the inner region ($\lesssim 0.6$ AU).

In the previous chapter, we found that the planetesimal disk gap retards the migration

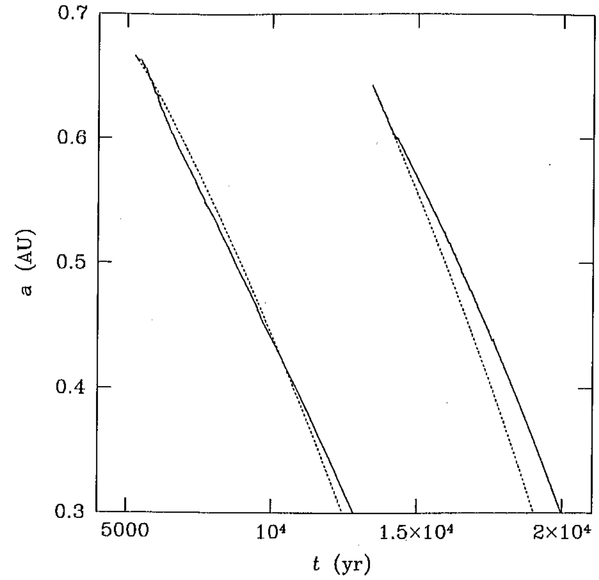

Figure 3.3: Semimajor axis evolution of the largest protoplanet that emerged at $t \sim 5000$ years (left lines) and $t \sim 1.3 \times 10^4$ years (right lines) in Run4. The dotted lines are the analytical estimates that are drawn using $\tau_{\rm grav,mig}$. The solid lines are the N-body simulation results.

during the gap exists in the planetesimal disk, because a protoplanet seed with 1000 times larger mass than the individual planetesimal mass was placed initially. In the simulations in the present paper, we follow the growth of the protoplanets from the planetesimals. Since the formation time scale of the other large protoplanets is comparable with that of the largest protoplanet, such a gap can not be formed. The migration time scale is shorter with smaller a. Since the size of the protoplanets is comparable, the migration speed of the inner protoplanets tends be faster than or comparable with that of the outer ones. Hence, they move to the central star almost as if each protoplanet is placed alone in a disk.

3.2.2 Effects from the Outer Bodies

In the present paper, we carried out global calculations in order to study the effects from protoplanets and planetesimals supplied from outer regions as well. First, we check the outer boundary effect. In Run3, 4, and 5, the simulation parameters are the same, except for the outer boundary $a_{\rm max}$ (Table III). The final large protoplanets (with $m_{\rm p} > 0.1 M_\oplus$) that are left in 0.5-1.5 AU at $t = 10^6$ years have an average mass $m_{\rm p,end} = 0.35 M_\oplus, 0.56 M_\oplus$ and $0.60 M_\oplus$ in Run3, Run4 and Run5, respectively (Table IV). The significantly lighter $m_{\rm p,end}$ in Run3 suggests that a disk with the outer edge at 2 AU is too narrow. We will use the results only with outer boundary of 3AU or more, when we discuss the end results.

Figure 3.4 (a) shows the evolution of the semimajor axis of the largest protoplanet that has grown in relatively outer region in Run4 form 3×10^5-5×10^5 years. The dotted line is the analytical estimate based on $\tau_{\rm grav,mig}$, and the solid line is the result of Run4. As the gas dissipates ($\tau_{\rm dep} = 10^5$ years), the migration slows down. We have already shown that the inward migration is not effected by the inner protoplanets and the planetesimals. The agreement between the analytical estimate and the N-body simulation result in Fig.3.4 (a) suggests that the bodies from the outer regions do not affect the migration either.

Figure 3.4 (b) shows the mass evolution of the protoplanet in Fig.3.4 (a). The dotted line is the analytical evolution that is given by Tanaka and Ida (1999) assuming a protoplanet migrating alone in a planetesimal disk. For the inclination in the formula, equilibrium inclination in a gas disk (Kokubo and Ida 2002) is used. The N-body simulation result agrees well with the analytical line. It shows that the accretion during the migration is not affected by the other protoplanets and planetesimals supplied from the outer regions during this period.

3.2.3 Evolution of Solid Surface density and the Final Planets

The amount of solid material in the terrestrial planet region changes with time for the migration. Figure 3.5 (a) shows the evolution of solid surface density $\Sigma_{\rm s}$, averaged over the region of 0.6 - 1.5 AU in Run1, Run4, Run7 and Run10. The solid line is the N-body simulation result. The surface density $\Sigma_{\rm s}$ of solid components (planetesimals) is normalized with that of $\Sigma_{\rm s,SN}$ in that region. The four simulations that are listed here start with the same initial surface density $\Sigma_{\rm s,init} = 5\Sigma_{\rm s,SN}$, but with different $\tau_{\rm dep}$. The

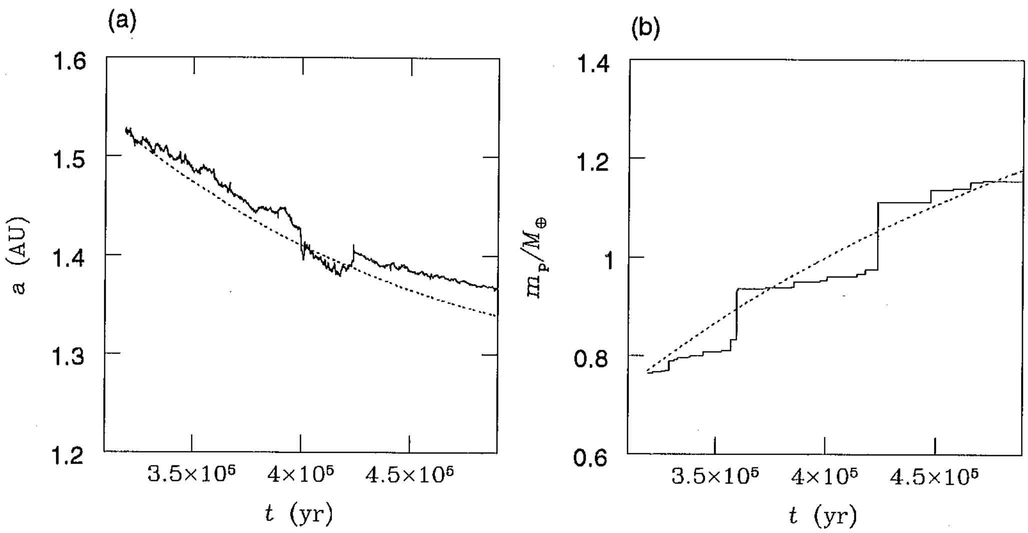

Figure 3.4: (a) Semimajor axis evolution of the largest embryo from $\sim 3 \times 10^5$ years to 5×10^5 years in Run4. The dotted lines are the analytical estimates that are drawn using $\tau_{\rm grav,mig}$. The solid lines are the N-body simulation results. (b) Mass evolution of the protoplanet depicted in (a). The dotted line is the analytical estimate from (3.15) and (3.20) in Tanaka and Ida (1999). Equilibrium inclination in a gas disk (Kokubo and Ida 2002) is used. The solid line is the N-body simulation result.

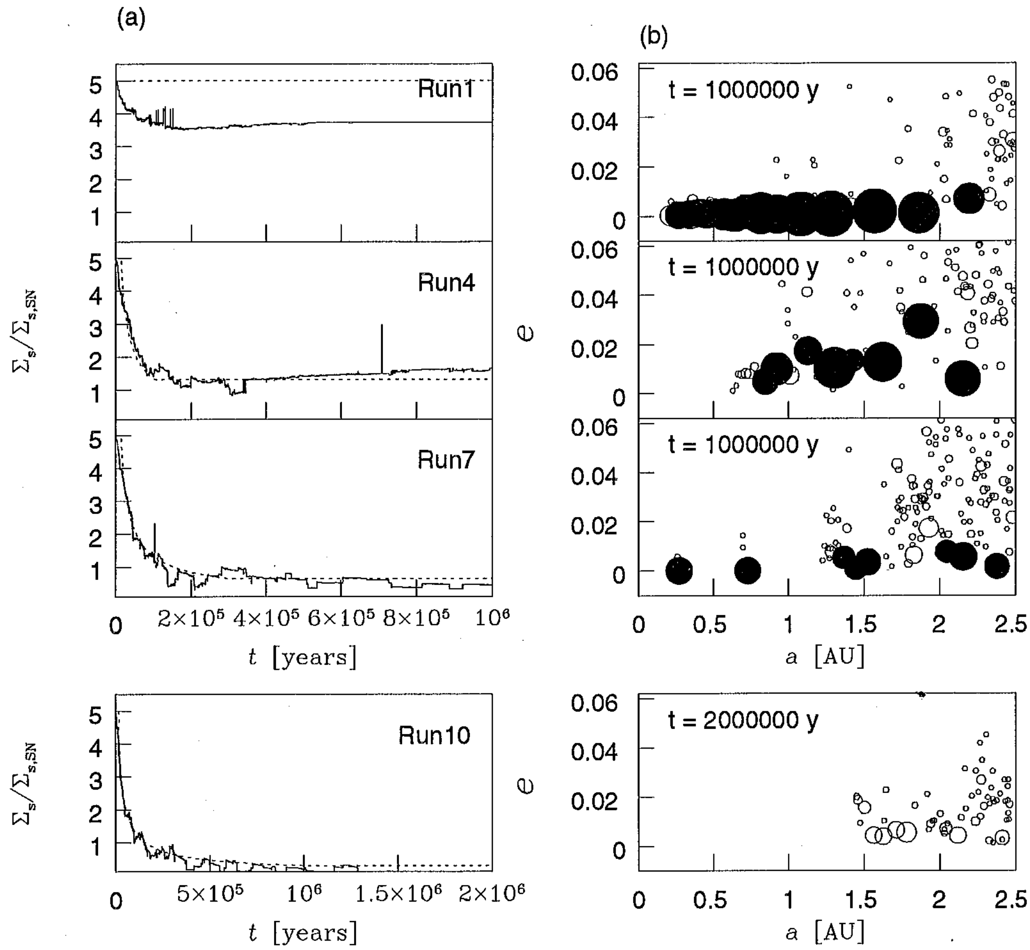

Figure 3.5: (a) Time evolution of solid surface density lies in the region of 0.6 AU $< a <$ 1.5 AU of Run1, Run4, Run7 and Run10. Gas depletion time scales are $\tau_{\rm dep} = 10^4, 10^5, 3 \times 10^5, 10^6$ years, respectively. The mass of planetesimals and the protoplanets in the region is added and normalized with the mass expected to exist in the same region of MMSN. Dotted lines are the analytical estimate (eq.(3.10)). The solid lines are the N-body simulation results. (b) Snap shots of Run1, Run4, Run7 and Run10 at $t = t_{\rm end}$, from the top. The descriptions of the dots are the same as in Fig.3.1.

depletion time scale for Run1, Run4, Run7 and Run10 is $\tau_{\rm dep} = 10^4, 10^5, 3 \times 10^5$ and 10^6 years, respectively. The solid lines decrease with time in not only the simulations that are presented in the figure, but also in other simulations.

The migration of the runaway protoplanets due to the gravitational drag in the inner region is faster than the planetesimal migration due to the aerodynamical gas drag. The migration time scale of a protoplanet at ~ 0.5 AU with $\sim 0.5 M_\oplus$ is $\tau_{\rm grav,mig} \sim 10^4$ years, while that of the planetesimals due to the gas drag is $\gtrsim 1.3 \times 10^6$ years. The runaway protoplanets grow and migrate to the central star leaving the planetesimals behind. The depletion of solid material in the disk is mainly due to the migration of the runaway protoplanets into the central star. As explained in the previous section, the formation and the migration proceed from the inner region, and the process is not affected by the supply of the protoplanets and planetesimals from the outer region. Hence, the solid surface density $\Sigma_{\rm s}$ decreases with time from the inner region.

For the longer depletion time scale, the amount of protoplanets that migrate to the central star is larger. As in Fig.3.4 (b), the growth rate is not affected much by the outer supply of protoplanets and planetesimals. Hence, the final $\Sigma_{\rm s}$ at $t = t_{\rm end}$ decreases with increase in $\tau_{\rm dep}$ as shown in Fig.3.5 (a). The final surface densities of all runs are listed in Table IV. The time $t_{\rm end}$ is determined so that the migration time scale for the bodies with $m_{\rm p} > 0.1 M_\oplus$ in 0.5-1.5 AU at $t_{\rm end}$ ($\tau_{\rm mig,end}$) longer than $\tau_{\rm dep}$ and $\Sigma_{\rm s}$ does not decrease significantly any more. Figure 3.5 (b) shows the protoplanets and planetesimals remaining at $t = t_{\rm end}$. The final planets are larger for the shorter depletion time scale because final $\Sigma_{\rm s}$ is larger. The average mass of the protoplanets with $m > 0.1 M_\oplus$ is listed in Table IV as well. The trend that larger protoplanets remain in the disk with shorter migration time scale is apparent.

3.2.4 Analytical Model for the Evolution of Solid Surface Density

In order to explain the time evolution of the solid surface density, we construct an analytical model. Since we found out that the growth and the migration are not affected by the interactions between the protoplanets and by the the torque from the planetesimal disk, the decrease of solid material can be described by using the linear solution. The migration time scale $\tau_{\mathrm{grav,mig}}$ is a function of the protoplanet's mass m_{p} and the semimajor axis a_{p}, as in eq.(2.12). If the protoplanet's mass is large enough to satisfy

$$t > \tau_{\mathrm{grav,mig}}(m_{\mathrm{p}}, a_{\mathrm{p}}), \tag{3.3}$$

the protoplanet falls to the central star. When the time t is longer than the gas depletion time scale, the above equation is replaced by

$$\tau_{\mathrm{dep}} > \tau_{\mathrm{grav,mig}}(m_{\mathrm{p}}, a_{\mathrm{p}}), \tag{3.4}$$

because considerable amount of gas is depleted and major migration ceases when $t > \tau_{\mathrm{dep}}$. The protoplanet's mass that satisfies

$$t = \tau_{\mathrm{grav,mig}}(m_{\mathrm{p}}, a_{\mathrm{p}}), \tag{3.5}$$

is the maximum mass $m_{\mathrm{p,max}}$ that survives in the disk at a_{p}. If the time t is longer than the depletion time scale τ_{dep},

$$\tau_{\mathrm{dep}} = \tau_{\mathrm{grav,mig}}(m_{\mathrm{p}}, a_{\mathrm{p}}) \tag{3.6}$$

gives the $m_{\mathrm{p,max}}$ at a_{p}.

When the mass of the protoplanet m_{p} exceeds $m_{\mathrm{p,max}}$, it falls to the central star. As the protoplanets fall, the solid surface density Σ_{s} decreases. New protoplanets are formed in the disk with decreased Σ_{s}. If the new protoplanets reach the mass of $m_{\mathrm{p,max}}$ again, they migrate to the central star. As the Σ_{s} decreases, the newly formed protoplanets' mass decreases as well. Eventually Σ_{s} reaches a point where the protoplanets can not reach $m_{\rm p,max}$. Then the decrease of $\Sigma_{\rm s}$ stops. Because $m_{\rm p,max}$ is a function of t and $a_{\rm p}$, the equilibrium $\Sigma_{\rm s}$ is given by t and $a(=a_{\rm p})$.

To derive such $\Sigma_{\rm s}$, a function to express $m_{\rm p}$ with $\Sigma_{\rm s}$ is needed. We first estimate $m_{\rm p}$ to be an isolation mass (Kokubo and Ida 2002)

$$m_{\rm p} = m_{\rm iso}(\Sigma_{\rm s}, a_{\rm p}) = 0.093 \left(\frac{\Sigma_{\rm s} f_{\rm ice}}{\Sigma_{\rm s,SN}}\right)^{3/2} \left(\frac{a_{\rm p}}{1{\rm AU}}\right)^{3/4} M_{\oplus}, \tag{3.7}$$

where we assume that the separation between the protoplanets is 10 times their mutual Hill radius

$$r_{\rm m,H} = \left(\frac{2m_{\rm p}}{3M_{\odot}}\right)^{1/3} a. \tag{3.8}$$

The isolation mass is derived assuming the protoplanet accretes all the planetesimals that reside within $10 r_{\rm m,H}$ around the protoplanet. We use it as a typical mass for runaway bodies in a disk with $\Sigma_{\rm s}$ at $a_{\rm p}$. Substituting $m_{\rm iso}$ into $\tau_{\rm grav,mig}$, we obtain the migration time scale for isolation mass,

$$\tau_{\rm grav,mig}(m_{\rm iso}, a_{\rm p}) = 7.5 \times 10^5 \left(\frac{\Sigma_{\rm s} f_{\rm ice}}{\Sigma_{\rm s,SN}}\right)^{-3/2} \left(\frac{a_{\rm p}}{1{\rm AU}}\right)^{3/4} \left(\frac{\Sigma_{\rm g}}{\Sigma_{\rm g,SN}}\right)^{-1} \tag{3.9}$$

Applying eq.(3.9) for eqs.(3.5) and (3.6), we obtain the equilibrium solid surface density as a function of t and $a(=a_{\rm p})$,

$$\left(\frac{\Sigma_{\rm s} f_{\rm ice}}{\Sigma_{\rm s,SN}}\right) = \begin{cases} \frac{\Sigma_{\rm s,init} f_{\rm ice}}{\Sigma_{\rm s,SN}} & [t < t_*] \\ \left(\frac{t}{7.5\times 10^5 {\rm yr}}\right)^{-2/3} \left(\frac{\Sigma_{\rm g}}{\Sigma_{\rm g,SN}}\right)^{-2/3} \left(\frac{a}{1{\rm AU}}\right)^{1/2} & [t > t_*] \end{cases} \tag{3.10}$$

where

$$t_* = 7.5 \times 10^5 \left(\frac{\Sigma_{\rm s,init} f_{\rm ice}}{\Sigma_{\rm s,SN}}\right)^{-3/2} \left(\frac{\Sigma_{\rm g}}{\Sigma_{\rm g,SN}}\right)^{-1} \left(\frac{a}{1{\rm AU}}\right)^{3/4} {\rm years}. \tag{3.11}$$

Protoplanets can start the migration before $m_{\rm p}$ reaches $m_{\rm iso}$, and

$$m_{\rm p} = m_{\rm p}(t, \Sigma_{\rm s}, a_{\rm p}) \tag{3.12}$$

should be used for eqs.(3.5) and (3.6). In other words, the condition

$$t = \tau_{\rm growth} \tag{3.13}$$

is used to evaluate m_p. Since we consider the mass of protoplanets that undergo major migration,

$$\tau_\mathrm{dep} = \tau_\mathrm{growth}. \tag{3.14}$$

is used when $t > \tau_\mathrm{dep}$. If t is large and the protoplanets have already grown to the mass close to m_iso, eq.(3.7) is suitable. However, when t is small and the protoplanets have not grown enough, eq.(3.12) is more appropriate to evaluate $m_\mathrm{p,max}$. The specific equations of Σ_s using eqs.(3.12) and (3.5) are derived in the Appendix.

The analytical estimate of Σ_s derived using eq.(3.5) and eq.(3.7) is plotted in Fig.3.5 (a) in dotted lines, assuming $a_\mathrm{p} = 1$ AU. The N-body simulation results are the averaged value of Σ_s over 0.6 - 1.5AU as explained previously. Since the physical radius enhancement is $f = 5$ in the simulations, the protoplanets around 1AU grows quickly to $\sim m_\mathrm{iso}$. Hence, the N-body results averaged over the region near 1AU match the analytical estimate using m_iso well. Note that in Run1, the analytical line does not drop from the initial value. The depletion time scale is shorter than the migration time scale for the isolation mass in the disk with $\Sigma_\mathrm{s,init} = 5.0\Sigma_\mathrm{s,SN}$.

The time averaged value of final $\Sigma_\mathrm{s}/\Sigma_\mathrm{s,SN}$ of each of the simulations is listed in Table IV. The analytical value $\Sigma_\mathrm{s,AN}/\Sigma_\mathrm{s,SN}$ is derived using eqs.(3.5) and (3.7). They agree with each other within a factor 2 except for Run9 and Run10. Note that $\Sigma_\mathrm{AN}/\Sigma_\mathrm{s,SN}$ in Run9 and Run10 is fairly small. Since the planetesimal size is relatively large, the simulations are not sensitive enough to express such a small surface density. Except for such cases, the trend that smaller amount of material remains in the disk with longer depletion time scales is apparent.

Figure 3.6 shows the snapshots of Σ_s evolution on Σ_s-a plane. The dots are the N-body simulation result in Run4 ($\tau_\mathrm{dep} = 10^5$ years). We divided the simulation area with separations of Δa =0.2AU, smoothed out the mass distribution of the planetesimals in that region to evaluate Σ_s. The evaluated Σ_s is normalized with $\Sigma_\mathrm{s,SN}$. Since formation and migration of runaway bodies start from the inner region of the disk, Σ_s decreases

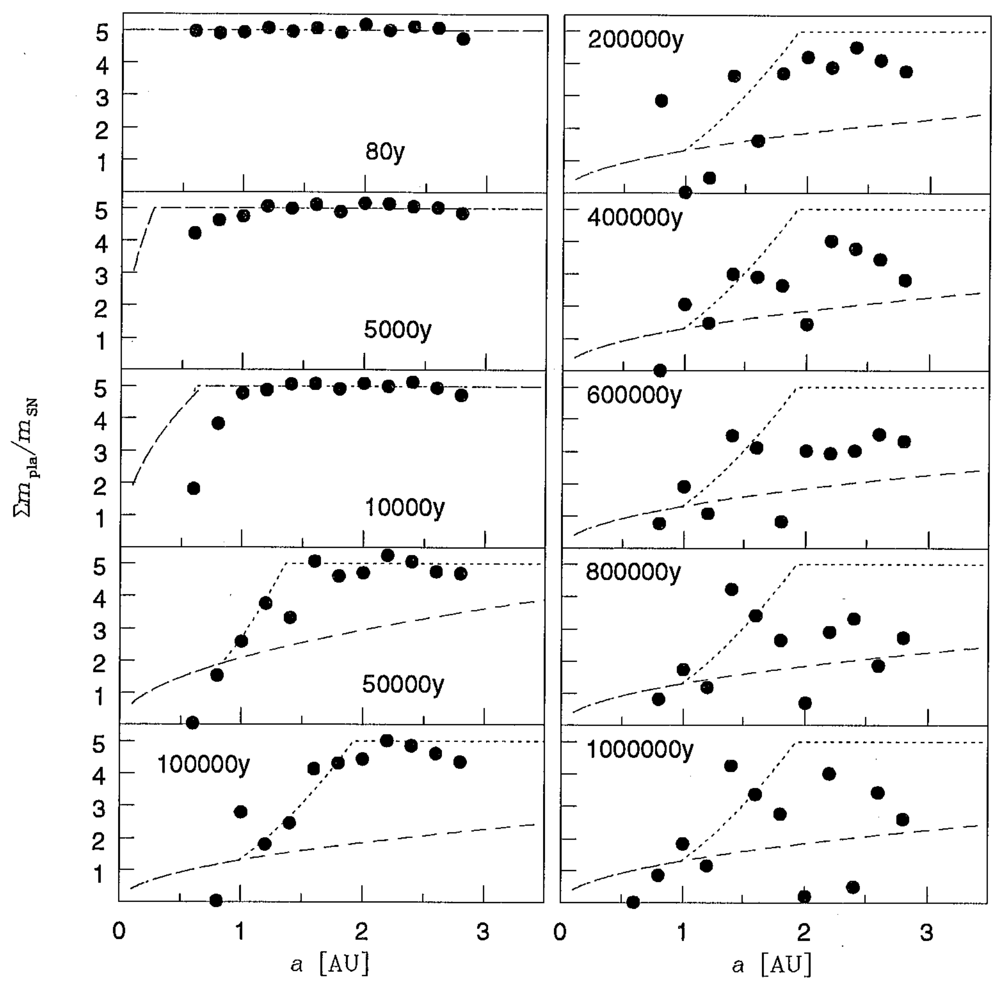

Figure 3.6: Time evolution of solid surface density of Run4. The snapshots of Σ_s through out the region. The solid dots are the N-body simulation results. The simulation area is divided with separation of 0.2AU. All the mass in the area is added and normalized with the mass that should exist if MMSN is assumed. The dotted line is the analytical estimate by eq(6.6) and eq(3.10). The dashed line is the estimate of eq(3.10), assuming $m_{\rm iso}$ only. When $t < \tau_{\rm dep}$, simulation time is used, and when $t > \tau_{\rm dep}$, $\tau_{\rm dep}$ is used for the time.

from the inner region. The dotted line is the analytical estimate derived by the condition eq.(3.5) with $m_{\rm p}$ given by eq.(3.12). When $t > \tau_{\rm dep}$, the condition eq.(3.6) is used. The dashed line is plotted using the condition eq.(3.5) (eq.(3.6) for $t > \tau_{\rm dep}$) with $m_{\rm iso}$ given by eq.(3.7). At $a \gtrsim 1.5$ AU, since growth of protoplanets is relatively slow and their mass does not reach $m_{\rm iso}$ on the time scale comparable to $\tau_{\rm dep}$, the dotted line with $m_{\rm p}(t)$ fits better with the N-body simulation results than the dashed line with $m_{\rm iso}$. However, since the growth is relatively fast at $a \sim 1$AU, the estimate with $m_{\rm iso}$ also gives a good approximation there. If longer $\tau_{\rm dep} = 10^6 - 10^7$ years, which is more consistent with the observationally inferred one, is adapted, the estimate with $m_{\rm iso}$ is applicable for $\Sigma_{\rm s}$ in more outer regions at $t \gtrsim \tau_{\rm dep}$. Note that the solid material of outer region continues to decrease, due to diffusion of material to outer region. The disk expands to ~ 3.5 AU in this case. If wider disks are considered, such diffusion would not be apparent and the area that the analytical line being valid would become wider. Hence, the decrease of material in outer region is irrelevant.

Since eq.(3.12) changes with the physical radius enhancement f and the strength of the aerodynamical gas drag, the estimate with $m_{\rm p}(t)$ has numerous parameters. As shown in Fig.3.5(a), Table IV and Fig.3.6, the solid surface density left in the terrestrial planet region after the gas depletion time scale is approximated by the estimate with $m_{\rm iso}$ within a factor ~ 2. Hereafter, we will use the simple estimate with $m_{\rm iso}$ in this chapter.

As shown in above, the N-body results are consistent with the analytical formula that assumes the migration time scale for one independent protoplanet in a gas disk migrating toward the central star and the growth rate without the effect of other protoplanets and planetesimals supplied from outer regions. These agreement reconfirms the result in section 3.2.1 and 3.2.2.

The final disk solid mass also depends on the initial disk mass. Run4 and Run6 have the same gas depletion time scale $\tau_{\rm dep} = 10^5$ years, but differ in initial disk surface density (Table III). Run4 starts with $\Sigma_{\rm s} = 5\Sigma_{\rm s,SN}$ and Run5 starts with $10\Sigma_{\rm s,SN}$. Table IV shows

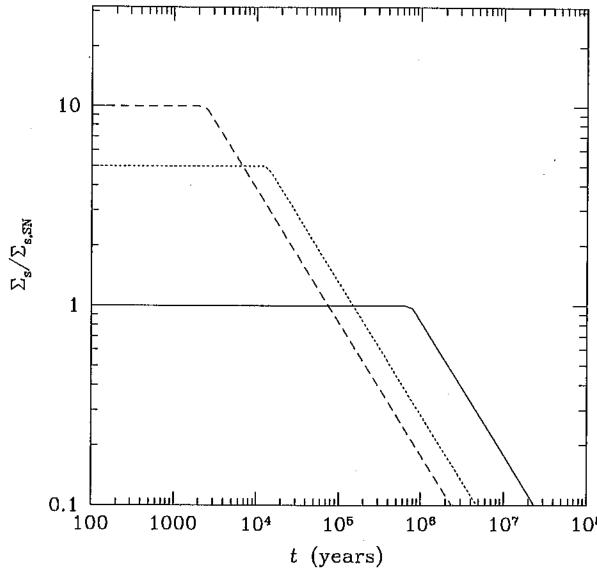

Figure 3.7: Analytical solid surface density evolution $\Sigma_s/\Sigma_{s,SN}$, using eq(3.10) at 1AU. The solid line is for the disk with initial gas and dust surface density of $1\Sigma_{SN}$, the dotted line is for $5\Sigma_{SN}$ and the dashed line is for $10\Sigma_{SN}$.

that the amount of solid material left in the disk in the terrestrial region is larger in Run4. The same result is obtained by comparing Run7 and Run8. The larger the initial disk material is, the less solid material remains. Figure 3.7 shows how Σ_s at 1AU evolves using eq.(3.10). The solid, dotted and dashed lines are with initial dust surface density $\Sigma_{s,init} = \Sigma_{s,SN}, 5\Sigma_{s,SN}$ and $10\Sigma_{s,SN}$. Since we fix the gas to dust ratio, Σ_g is proportional to $\Sigma_{s,init}$ disks. In larger $\Sigma_{s,init}$ disks, Σ_s starts to decrease earlier (eq.(3.11)), since more massive protoplanets having shorter $\tau_{grav,mig}$ are formed in these disks. Even after $\Sigma_s(t)$ declines, Σ_s decreases earlier in initially heavier disks than in disks with the same Σ_s(t) and smaller $\Sigma_{s,init}$, because larger Σ_g in these disks results in shorter $\tau_{grav,mig}$. Our N-body simulations show the consistent results. Note that in the results in Fig.3.7, the size of the planets is *larger* in *smaller* $\Sigma_{s,init}$ disks after $t = 10^5$ years. The planets' size may not indicate the initial disk mass if the effect of migration is included.

3.2.5 Conditions to Retain Solid Surface Density of MMSN

Our simulation showed that the interactions with other protoplanets and planetesimals, do not moderate the migration of a protoplanet. The accretion and migration of the protoplanet proceed in the same way as if it is placed in a gas disk alone. We showed that solid surface density remaining after the gas dissipation is given by $\Sigma_{\rm s}$ with $t = \tau_{\rm dep}$ as

$$\left(\frac{\Sigma_{\rm s} f_{\rm ice}}{\Sigma_{\rm s,SN}}\right) = \begin{cases} \frac{\Sigma_{\rm s,init} f_{\rm ice}}{\Sigma_{\rm s,SN}} & [t < t_*] \\ \left(\frac{t}{7.5\times 10^5 {\rm yr}}\right)^{-2/3} \left(\frac{\Sigma_{\rm g}}{\Sigma_{\rm g,SN}}\right)^{-2/3} \left(\frac{a}{1{\rm AU}}\right)^{1/2} & [t > t_*] \end{cases} \tag{3.10}$$

where $\Sigma_{\rm g}$ is the initial gas surface density and

$$t_* = 7.5 \times 10^5 \left(\frac{\Sigma_{\rm s,init} f_{\rm ice}}{\Sigma_{\rm s,SN}}\right)^{-3/2} \left(\frac{\Sigma_{\rm g}}{\Sigma_{\rm g,SN}}\right)^{-1} \left(\frac{a}{1{\rm AU}}\right)^{3/4}. \tag{3.11}$$

Using this formula, we can impose some constraints on migration speed and $\tau_{\rm dep}$ in order to retain specific amount of $\Sigma_{\rm s}$.

In particular, we consider the range of migration speed and $\tau_{\rm dep}$ to retain $\Sigma_{\rm s,SN}$ to reproduce our solar system. We introduce a parameter $A_{\rm mig}$ for migration speed as

$$\tau_{\rm grav,mig} = A_{\rm mig} 7.0 \times 10^4 \left(\frac{m_{\rm p}}{M_\oplus}\right)^{-1} \left(\frac{a}{1{\rm AU}}\right)^{3/2} \left(\frac{\Sigma_{\rm s,init} f_{\rm ice}}{\Sigma_{\rm s,SN}}\right)^{-1} \text{ years.} \tag{3.15}$$

where

$$A_{\rm mig} = C \left(\frac{\Sigma_{\rm g,init}/\Sigma_{\rm s,init} f_{\rm ice}}{\Sigma_{\rm g,SN}/\Sigma_{\rm s,SN}}\right)^{-1}, \tag{3.16}$$

and C expresses a deviation factor from the result of linear calculation (Tanaka et al. 2002). If other effects such as gas turbulence or radiative transfer exist, C can take a value other than unity. The parameter $A_{\rm mig}$ is a function of gas to dust ratio normalized with that of MMSN. Using eq.(3.15), eq(3.10) reads as

$$\left(\frac{\Sigma_{\rm s} f_{\rm ice}}{\Sigma_{\rm s,SN}}\right) = \begin{cases} \frac{\Sigma_{\rm s,init} f_{\rm ice}}{\Sigma_{\rm s,SN}} & [t < t_*] \\ A_{\rm mig}^{2/3} \left(\frac{t}{7.5\times 10^5 {\rm yr}}\right)^{-2/3} \left(\frac{a}{1{\rm AU}}\right)^{1/2} \left(\frac{\Sigma_{\rm s,init} f_{\rm ice}}{\Sigma_{\rm s,SN}}\right)^{-2/3} & [t > t_*] \end{cases} \tag{3.17}$$

where

$$t_* = A_{\rm mig} 7.5 \times 10^5 \left(\frac{\Sigma_{\rm s,init} f_{\rm ice}}{\Sigma_{\rm s,SN}}\right)^{-5/2} \left(\frac{a}{1{\rm AU}}\right)^{3/4}. \tag{3.18}$$

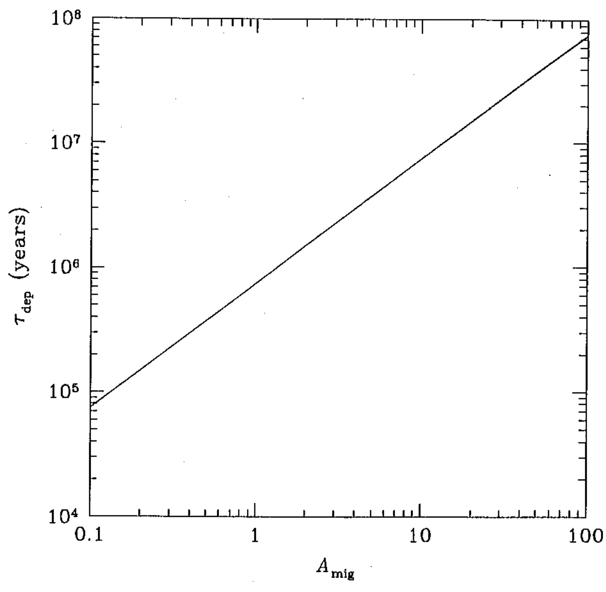

Figure 3.8: Analytical estimate for the gas depletion time scale $\tau_{\rm dep}$ as a function of $A_{\rm mig}$, using eq(3.15). Disks with the parameters below the line can retain $\Sigma_{\rm s} > \Sigma_{\rm s,SN}$ at 1AU.

In order to leave a solid surface density of $\Sigma_{\rm s,crit}$, $\tau_{\rm dep}$ should be

$$\tau_{\rm dep} = A_{\rm mig} 7.5 \times 10^5 \left(\frac{\Sigma_{\rm s,crit} f_{\rm ice}}{\Sigma_{\rm s,SN}}\right)^{-3/2} \left(\frac{a}{1{\rm AU}}\right)^{3/4} \left(\frac{\Sigma_{\rm s,init} f_{\rm ice}}{\Sigma_{\rm s,SN}}\right)^{-1} \text{years.} \tag{3.19}$$

For $\Sigma_{\rm s,crit} = \Sigma_{\rm s,SN}$ at $a = 1$ AU, the relation between $\tau_{\rm dep}$ and $A_{\rm mig}$ is shown in Figure 3.8. Disks with parameters below the line can retain $\Sigma_{\rm s} > \Sigma_{\rm s,SN}$. The observationally inferred $\tau_{\rm dep}$ is $\sim 10^6 - 10^7$ years. For these values of $\tau_{\rm dep}$, $1.3 \lesssim A_{\rm mig} \lesssim 13$. If $A_{\rm mig} = 1$, $\tau_{\rm dep}$ should be $\sim 7 \times 10^5$ years, which is too short to make terrestrial planets with small eccentricity. There will be not enough gas left to damp the pumped up eccentricity due to the orbital crossing after the planets are formed (Kominami and Ida 2002, 2004). Since $A_{\rm mig}$ is a function of the initial gas to dust ratio, the condition $1.3 \lesssim A_{\rm mig} \lesssim 13$ can be obtained by reducing the initial amount of gas and changing the initial gas to dust ratio. So far, we have assumed that the gas to dust ratio $(\Sigma_{\rm g}/\Sigma_{\rm s})$ is fixed as $\Sigma_{\rm g,SN}/\Sigma_{\rm s,SN} \sim 240$. However, gas to dust ratio can be altered by the migration of the dust and planetesimals due to gas drag. Hence, it needs not to be fixed to ~ 240. If the initial gas to dust ratio is $\lesssim 0.75(\Sigma_{\rm g,SN}/\Sigma_{\rm s,SN})$, $A_{\rm mig} \gtrsim 1.3$ even if $C = 1$. Then, disks with $\tau_{\rm dep} \simeq 10^6$ years can

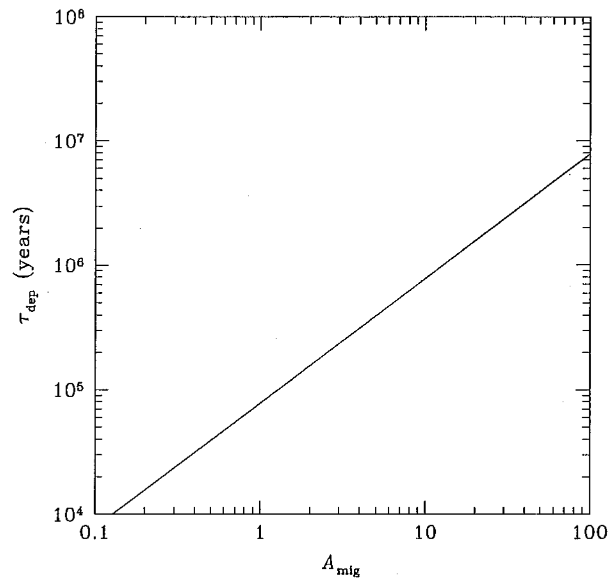

Figure 3.9: The same description for the lines as in Figure 3.8, except $a = 5$ AU.

retain solid material of $\sim \Sigma_{\rm s,SN}$.

The formula we have obtained can be used at $a = 5$ AU as well. Substituting $f_{\rm ice} = 4, \Sigma_{\rm s,crit} = \Sigma_{\rm s,SN}$ and $a = 5$ AU into eq.(3.19), we obtain $\tau_{\rm dep} = 8.0 \times 10^4 A_{\rm mig}$ years (Fig.3.9). If $A_{\rm mig} \sim 1$, $\tau_{\rm dep} \lesssim 10^5$ years, which is too short to form a core with several Earth masses. If the depletion time scale is 10^6-10^7 years, $A_{\rm mig}$ should be $\sim$ 13-130. The gas to dust ratio smaller than at least $\sim 0.1(\Sigma_{\rm g,SN}/\Sigma_{\rm s,SN})$ is needed at ~ 5 AU to from a core that can start runaway gas accretion there, if $C = 1$.

3.3 Summary

In this chapter, we investigated how the migration due to disk-planet interaction (type-I migration) of the runaway bodies and the disk evolution proceed as the disk gas dissipates. We study the evolution of systems with multiple protoplanets in a dissipating gas disk, by carrying out global simulations with initially wider disks (0.5 - 3 AU) than in the simulations in the previous chapter. Since we start with the planetesimals with equal mass without a seed, multiple large protoplanets emerge in the disks, interacting with one another.

Ten simulations are carried out (Run1 - 10). The parameters are the gas depletion time scale $\tau_{\rm dep}$, and the initial disk surface density $\Sigma_{\rm s,init}$. The summary of the results are the following.

1. Because the time scale for the runaway growth and migration of protoplanets to occur, rapidly increases with semimajor axis, they are not affected by other protoplanets' existence. The inner protoplanets are already gone by the migration toward the central star, and the outer ones are not grown enough to migrate inward. Using this result, we constructed an analytical model for the solid surface density evolution under the assumption that a body in a gas disk migrate alone without being affected by other bodies. The results from the N-body simulations are in good agreement with the analytical model.
2. The smaller amount of solid material remains in the disk as the gas depletion decreases with increase in $\tau_{\rm dep}$ and $\Sigma_{\rm s,init}$. For longer $\tau_{\rm dep}$, more protoplanets that are large enough to undergo migration are formed. They have enough time to migrate by significant distance.
3. A strange dependence on $\Sigma_{\rm s,init}$ comes from the assumption of the fixed gas to dust ratio. The migration is more effective in larger $\Sigma_{\rm s,init}$ cases, because the disk contains larger amount of gas. The final protoplanets' mass is determined by the $\Sigma_{\rm s}$ after the gas depletion. Hence, large planets are not necessarily made in initially heavy disks.

By analyzing the formula we derived, the following possibilities can be considered in order to retain $\Sigma_{\rm s} \gtrsim \Sigma_{\rm s,SN}$.

1. *The gas depletion time scale is shorter than the observational value.*

Our formula shows that the depletion time scale needs to be $\lesssim 7.5 \times 10^5$ years, around 1AU. Although the observation implies the gas depletion time scale to be $\sim 10^6 - 10^7$ years, such implication is obtained by observing the outer region of the disk such as $\sim$ 100 AU. Hence, the depletion time scale in terrestrial planet region may be less than the observational value. However, if this is so, the eccentricity of the final planets will be high; not enough gas will remain in the disk to damp the random velocity, after the giant impact stage. The amount of the gas needed to damp the final planets is $\sim 10^{-4}\Sigma_{\rm g,H}$ (Kominami and Ida 2002, Agnor and Ward 2002). It is unlikely for the disk to lose the large amount of the gas in such a short period in the first place, and retain such a small amount during the next 10^7 years. Unless there is such a mechanism, considering a short depletion time scale is contradictory. In the Jovian planet region, our formula shows that the depletion time scale should be $\lesssim 10^5$ years. The time scale for a giant planet to form $T_{\rm giant}$ is

$$T_{\rm giant} = T_{\rm core} + T_{\rm acc}, \tag{3.20}$$

where $T_{\rm core}$ is the time scale for the core to form, and the $T_{\rm acc}$ is the accretion time scale for the core to accrete the gas to form a gas giant planet. Supposing the size of the core that starts the runaway gas accretion is $\sim 5M_\oplus$; $T_{\rm core}$ is $\sim 2 \times 10^7$ years (Kokubo and Ida 2002). In order for $T_{\rm core}$ to be smaller, core mass has to be smaller. On the other hand, if the mass of the core is small, the gas accretion time scale ($T_{\rm acc}$) becomes long. Hence, it is hard to make $T_{\rm giant}$ be within $\sim 10^5$ years. Moreover, if the gas is depleted in a short time scale, there will be not enough gas for the cores to accrete. Hence, short depletion time scale of disk gas may be contradictory .

2. *The migration speed is slower at least by factor of several times than the speed given by the linear theory.*

By introducing retardation factor as in eq.(3.15), we constrain the migration time scale for the disk to retain one minimum disk solid material. If the observational inferred disk gas depletion time scale $\tau_{\mathrm{dep}} \sim 10^6$ years is assumed, the retardation should be more than $A_{\mathrm{mig}} \sim 1.3$ around 1AU and $A_{\mathrm{mig}} \sim 13$ around 5AU. By considering the effects such as turbulence in the gas disk and/or radiative transfer, the factor C in eq.(3.15) can be altered, and these values of retardation factor may be able to be reached in MMSN.

3. *The gas to dust ratio at the beginning of the accretion is less than that of MMSN, assuming $\tau_{\mathrm{dep}} \sim 10^6$ years.*

The retardation factors $A_{\mathrm{mig}} \sim 1.3$ around 1AU and $A_{\mathrm{mig}} \sim 13$ around 5AU can also be reached by by decreasing the amount of initial gas to dust ratio by factor ~ 1.3 and ~ 13 at 1AU and 5AU respectively from that of MMSN ($\Sigma_{\mathrm{g,SN}}/\Sigma_{\mathrm{s,SN}}$). The ratio can be altered by the migration of dust and planetesimals in the disk during the planetesimal formation stage. It needs not to be the same as that in MMSN when the accretion of the planetesimals start. Hence, if the ratio is less than that in MMSN by factor ~ 10, $\Sigma_{\mathrm{s,SN}}$ and be retained.

3.4 Tables

Table III

Simulation Parameters of Run1-10

Run	$\tau_{\rm dep}$(years)	$\Sigma_{\rm s,init}/\Sigma_{\rm s,SN}$,$B_{\rm grav}$	$a_{\rm max}$(AU)	$m_{\rm pla}$ (g)	N
Run1	10^4	5	2	1.0×10^{25}	9969
Run2	10^4	10	2	3.0×10^{25}	6644
Run3	10^5	5	2	1.0×10^{25}	9969
Run4	10^5	5	3	1.5×10^{25}	9632
Run5	10^5	5	5	1.5×10^{25}	14370
Run6	10^5	10	3	4.0×10^{25}	7223
Run7	3×10^5	5	3	1.5×10^{25}	9632
Run8	3×10^5	10	3	4.0×10^{25}	7223
Run9	10^6	5	2	1.0×10^{25}	9969
Run10	10^6	5	3	1.5×10^{25}	9632

List of initial conditions and the parameters for the simulations. From the left column, Run is the name of the simulation, $\tau_{\rm dep}$ is the gas depletion time scale, $\Sigma_{\rm s,init}/\Sigma_{\rm s,SN}$ is the initial solid surface density, $B_{\rm grav}$ is the initial gravitational force. This parameter corresponds the initial gas surface density. In next column, $a_{\rm max}$ is the outer boundary of the planetesimal disk initially placed, $m_{\rm pla}$ is mass of each planetesimal and N is the initial number of the planetesimals.

Table IV

Final States of the Simulations of Run1-10

Run	$t_{\rm end}$(yrs)	$m_{\rm p,end}/M_\oplus$	$\tau_{\rm mig,end}$(years)	$\Sigma_{\rm s,AN}/\Sigma_{\rm s,SN}$	$\Sigma_{\rm s,end}/\Sigma_{\rm s,SN}$
Run1	10^6	1.14	2.6×10^{47}	5.0	3.73
Run2	10^6	1.78	1.9×10^{47}	3.8	6.14
Run3	10^6	0.352	1.5×10^9	1.3	0.840
Run4	10^6	0.563	1.1×10^9	1.3	1.59
Run5	10^6	0.601	6.6×10^9	1.3	1.65
Run6	10^6	0.724	3.6×10^8	0.8	1.10
Run7	10^6	0.300	1.1×10^6	0.6	0.423
Run8	10^6	0.307	8.9×10^5	0.4	0.333
Run9	2×10^6	0.053	1.3×10^6	0.3	0.0735
Run10	2×10^6	0.13	1.8×10^6	0.3	0.00459

The lists of final states of the simulations. From the left column, $t_{\rm end}$ is the end time of the simulation, $m_{\rm p,end}/M_\oplus$ is the average mass of the bodies with $> 0.1M_\oplus$ at $t = t_{\rm end}$ in 0.5-1.5

AU. In Run9 and Run10, the largest protoplanet mass is indicated. $\tau_{\rm mig,end}$ is the averaged migration time scale of bodies with $m_{\rm p} > 0.1 M_\oplus$ at $t = t_{\rm end}$ in 0.5-1.5 AU, $\Sigma_{\rm s,AN}/\Sigma_{\rm s,SN}$ is the analytical solid surface density at 1AU obtained by eq(3.10) and $\Sigma_{\rm s,end}/\Sigma_{\rm s,SN}$ is the final solid surface density of 0.6 - 1.5 AU in the simulation. Each value is averaged over 2×10^5 years.

Chapter 4

Discussion

In chapter 2 and chapter 3, we showed that the interaction between the protoplanet and the planetesimal disk, and between other protoplanets do not affect the migration process. The protoplanet falls to the central star as if it is placed in a gas disk alone. This result leads us to more general description of planetesimal disk depletion and evolution. Recently, various extra solar planetary systems have been discovered. Initial planetesimal disks do not have to be constrained to be similar to MMSN. Disks may have various surface densities. Here, we discuss the depletion of disk solid material more generally.

General Analytical Model

In our N-body simulations, radius was enhanced for computational reason. In such cases, the equilibrium eccentricity is obtained by equating τ_{growth} and τ_{VS} (eq.(6.4)). However, in the real world, there should be no enhancement. The eccentricity is obtained by equating aerodynamical gas drag time scale τ_{gas} and viscous stirring time scale τ_{VS} (Kokubo and Ida 2002). Specific derivation is described in the appendix. In the region where m_{p} does not reach m_{iso}, instead of eq.(3.10), following equation is applied for the solid surface density,

$$\left(\frac{\Sigma_{\mathrm{s}} f_{\mathrm{ice}}}{\Sigma_{\mathrm{s,SN}}}\right) = \begin{cases} \frac{\Sigma_{\mathrm{s,init}} f_{\mathrm{ice}}}{\Sigma_{\mathrm{s,SN}}} & [t < t_*] \\ 4 \times 10^7 \left(\frac{t}{1\mathrm{year}}\right)^{-4/3} \left(\frac{\Sigma_{\mathrm{g}}}{\Sigma_{\mathrm{g,SN}}}\right)^{-11/15} \left(\frac{a}{1\mathrm{AU}}\right)^{16/5} \left(\frac{m_{\mathrm{pla}}}{10^{20}\mathrm{g}}\right)^{2/15} & [t > t_*] \end{cases} \tag{4.1}$$

where

$$t_* = 5\times10^5\left(\frac{\Sigma_{\rm s,init}f_{\rm ice}}{\Sigma_{\rm s,SN}}\right)^{-3/4}\left(\frac{\Sigma_{\rm g}}{\Sigma_{\rm g,SN}}\right)^{-33/20}\left(\frac{a}{1{\rm AU}}\right)^{12/5}\left(\frac{m_{\rm pla}}{10^{20}{\rm g}}\right)^{1/10}\ {\rm years.} \tag{4.2}$$

We assumed $\rho_{\rm p} = 3{\rm g/cm}^3$ and $\tilde{b} = 10$. When the factor $A_{\rm mig}$ is used, eq.(4.1) changes to

$$\left(\frac{\Sigma_{\rm s}f_{\rm ice}}{\Sigma_{\rm s,SN}}\right) = \begin{cases} \frac{\Sigma_{\rm s,init}f_{\rm ice}}{\Sigma_{\rm s,SN}} & [t < t_*] \\ 4\times10^7 A_{\rm mig}^{1/3}\left(\frac{\Sigma_{\rm s,init}f_{\rm ice}}{\Sigma_{\rm s,SN}}\right)^{-1/3}\left(\frac{t}{1{\rm year}}\right)^{-4/3}\left(\frac{\Sigma_{\rm g,init}}{\Sigma_{\rm g,SN}}\right)^{-2/5}\left(\frac{a}{1{\rm AU}}\right)^{16/5}\left(\frac{m_{\rm pla}}{10^{20}{\rm g}}\right)^{2/15} & [t > t_*] \end{cases} \tag{4.3}$$

Incorporating initial gas to dust ratio $\gamma_{\rm init}$ and the initial solid surface density $\beta_{\rm init}$ as following,

$$\gamma_{\rm init} = \left(\frac{\Sigma_{\rm g,init}/\Sigma_{\rm s,init}f_{\rm ice}}{\Sigma_{\rm g,SN}/\Sigma_{\rm s,SN}}\right), \beta_{\rm init} = \frac{\Sigma_{\rm s,init}f_{\rm ice}}{\Sigma_{\rm s,SN}}, \tag{4.4}$$

the remaining solid surface density $\Sigma_{\rm s,fin}/\Sigma_{\rm s,SN} = \beta_{\rm fin}$ after $\tau_{\rm dep}$ can be written as following, depending on the mass of the protoplanet at $t = \tau_{\rm dep}$,

$$\beta_{\rm fin} = \begin{cases} 4\times10^7 C^{1/3}\beta_{\rm init}^{-11/5}\gamma_{\rm init}^{-11/5}\left(\frac{a}{1{\rm AU}}\right)^{16/5}\left(\frac{m_{\rm pla}}{10^{20}{\rm g}}\right)^{2/15}\left(\frac{\tau_{\rm dep}}{1{\rm year}}\right)^{-4/3} & [m_{\rm p} < m_{\rm iso}] \\ 8\times10^3 C^{2/3}\beta_{\rm init}^{-2/3}\gamma_{\rm init}^{-2/3}\left(\frac{a}{1{\rm AU}}\right)^{1/2}\left(\frac{\tau_{\rm dep}}{1{\rm year}}\right)^{-2/3} & [m_{\rm p} = m_{\rm iso}] \end{cases} \tag{4.5}$$

If other mechanism, such as turbulance is considered, factor C may become $C \neq 1$. Here we let $C = 1$, assuming type-I migration proceeds as the linear theory suggests. Using these more general equations, we can estimate how much disk solid material remains after the gas is depleted in various disks. For instance, Fig.4.1 shows the contour of $\beta_{\rm fin}$ on $\beta_{\rm init}$-$\gamma_{\rm init}$ plane at $t = \tau_{\rm dep} = 10^6$ years at 1AU. Disks with $\beta_{\rm init} = \gamma_{\rm init} = 0$, do not retain $\Sigma_{\rm s,SN}$ after the gas dissipates, as explained previously.

Solid Material Depletion in the Inner Region

The amount of remaining solid material depends on the depletion time scale as well as the semimajor axis. Figure4.2 shows the initial disk parameters that retains $\beta_{\rm fin} = 1$ when $10^6 < \tau_{\rm dep} < 10^7$ years at 0.3 AU. Assuming the depletion time scale is 10^6-10^7 years as indicated by the observation, little solid material remains in $a < 0.3$ AU. Although in MMSN, solid material increases as a becomes smaller even in small a region, this may not be true if type-I migration is considered. The fact that no planet exists inside the orbit of Mercury in our Solar system, may be due to type-I migration.

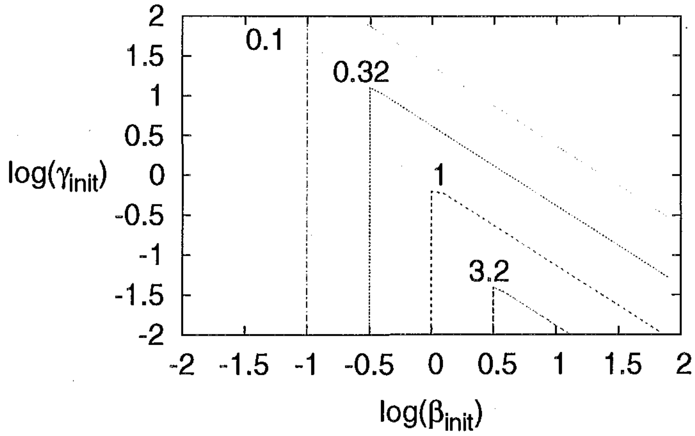

Figure 4.1: Contour of $\beta_{\rm fin}$ on $\beta_{\rm init}$-$\gamma_{\rm init}$ plane. Each number over the line indicates $\beta_{\rm fin}$ after $\tau_{\rm dep} = 10^6$ years at 1AU.

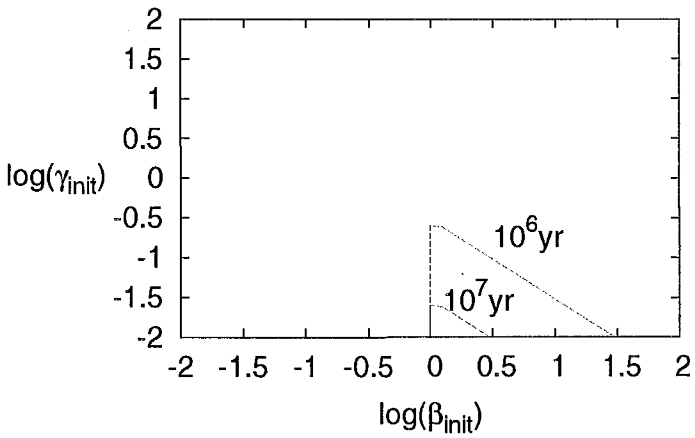

Figure 4.2: Contour of $\beta_{\rm fin} = 1$ on $\beta_{\rm init}$-$\gamma_{\rm init}$ plane at 0.3AU after 10^6 years and 10^7 years.

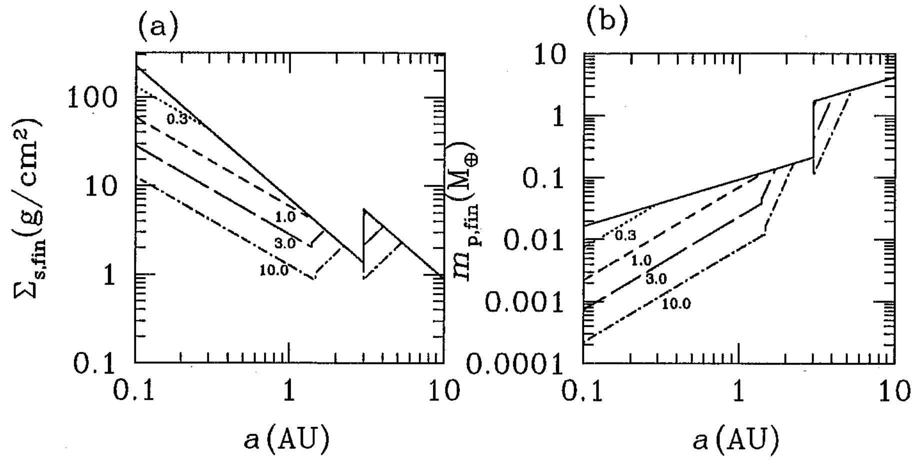

Figure 4.3: (a)Final $\Sigma_{\rm s,fin}$(g/cm^2) and (b)$m_{\rm p,fin}$ as function of a after $\tau_{\rm dep} = 10^6$ years with $\beta_{\rm init} = 1$. Solid line is drawn assuming MMSN without type-I migration. The dotted and dashed lines are drawn using various $\gamma_{\rm init}$ which is indicated below each line. $m_{\rm p,fin}$ in (b) is obtained using $\Sigma_{\rm s,fin}$ and eq.(3.7).

Comparison with MMSN

Kokubo and Ida (2002) studies the protoplanet distribution without type-I migration. Here we compare our results with their results and show how the solid material distribution differs from the case without considering type-I migration if it is included. Figure 4.3(a) shows the final solid surface density $\Sigma_{\rm s,fin}$(g/cm^2) as function of a AU after $\tau_{\rm dep} = 10^6$ years with $\beta_{\rm init} = 1$ with various initial gas to dust ratio $\gamma_{\rm init}$. The solid line is drawn assuming MMSN without type-I migration (Kokubo and Ida 2002). The dotted and dashed lines are below the solid line because the gas triggers type-I migration and depletion of solid material from the disk. As $\gamma_{\rm init}$ increases, the remaining material decreases. The profile of the disk in MMSN is $a^{-1.5}$. However, if type-I migration is included, it changes to a^{-1} at $a \lesssim 1.5$ AU. Surface density outside ~5 AU does not differ from MMSN. The growth and migration (hence, the depletion of solid material) proceeds from the inner region. If the depletion time scale is longer, remaining $\Sigma_{\rm s}$ will decrease even in the outer region. If $\tau_{\rm dep} = 10^7$ years, $\gamma_{\rm init} = 10$ line converges with line of MMSN at $\sim$ 15 AU.

Since the solid material in the inner region decreases more quickly than the outer region, the final mass distribution changes as well from that of MMSN, as in Fig.4.3(b). Figure 4.3(b) is obtained assuming the oligarchic growth takes place after $\tau_{\rm dep}$. Major depletion will not occur after the depletion time scale. The protoplanets grow to the isolation mass with $\Sigma_{\rm s,fin}(t = \tau_{\rm dep})$. Our results show that in the inner region, only small amount of surface density (hence, small planets) can be made, if gas to dust ratio of MMSN is considered. It is highly possible that initial plantesimal disk had different smaller gas to dust ratio and solid surface density from that of MMSN.

Habitable Planets in Habitable Zone

The mass of the final planets that are formed through the coagulation between the protoplanets can be estimated by assuming the feeding zone defined by escape velocity of the planets in the disk. The final mass turns out to be $\sim M_\oplus$ at $\sim$ 1 AU in the disk with $\Sigma_{\rm s,SN}$. Habitable zone in the disk with Solar mass central star lies between 0.95 AU to 1.37 AU (Kasting et al. 1993). The habitable planets mass is thought to be $\sim M_\oplus$ in order to keep the atmosphere. Hence, if disk with $\sim \Sigma_{\rm s,SN}$ remains, habitable planets can be formed at $\sim$ 1AU. With which disk parameter yields habitable planets in habitable zone, can be estimated using our formula. Figure 4.4 shows the disk parameter that retains $\beta_{\rm fin} = 1$ after $\tau_{\rm dep} = 10^6$-10^7 years at 1AU. The parameter region surrounded by the lines is where planets with $\sim M\oplus$ can survive at $\sim$ 1 AU. The planetesimal disks with small gas to dust ratio tends to yield habitable planets in habitable zone.

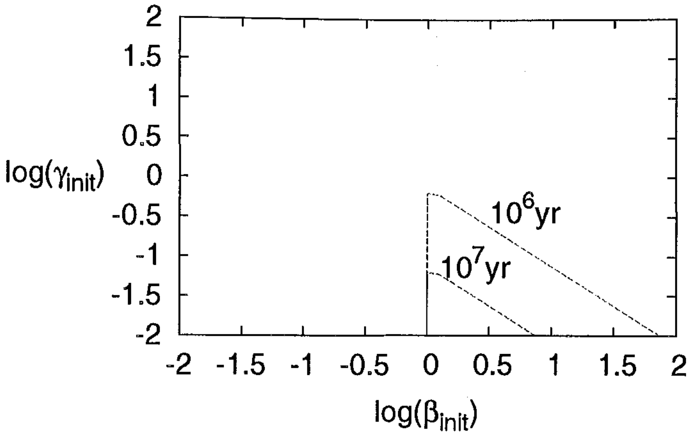

Figure 4.4: Contour of $\beta_{\rm fin} = 1$ on $\beta_{\rm init}$-$\gamma_{\rm init}$ plane after 10^6 years and 10^7 years at 1AU.

Chapter 5

Conclusion

Past N-body simulations on the formation of the protoplanets did not include the type-I migration effect for simplification. However, the linear calculation predicts the migration of the protoplanets with a shorter time scale than the gas depletion time scale, which is acquired from the observation. Terrestrial planets in our Solar system should have gone through such a migration stage. There has to be a mechanism for them to remain in the disk.

We examined the possible processes that would alter the migration speed. One is the gap formation in the planetesimal disk and the other one is the existence of multiple protoplanets. The planetesimal disk can prevent the migration by small factor temporarily, but not significantly enough to alter the migration time scale that is predicted by the linear calculation. The formation and migration of the protoplanets take place from the inner region of the disk. They grow and migrate as if they are placed in a gas disk alone. Effect from other protoplanets and planetesimals that migrate from behind turned out to be inefficient to change the migration time scale.

Our results show that if there is abundant gas in the disk, the migration that makes the planets fall to the central star is inevitable. The observational value of gas depletion time scale is $\sim 10^6$-10^7 years. However, the observed region of the disk is the outer realm of the disk ($\sim$ 100 AU). The gas depletion time scale of the terrestrial planet region may differ from such value. However, in order to damp the random velocity of the planets after the giant stage, there has to be small amount of gas left in the disk (Kominami and Ida 2002, 2004). The gas has to remain in the disk for more than million years. If the gas depletion is responsible for the stopping of the migration, there has to be a mechanism for the disk gas to dissipate significantly in first 10^5 years and to remain with small amount ($\sim 10^{-3}$-10^{-4} $\Sigma_{\rm g,SN}$) for million years.

If there is not such a mechanism, the migration mechanism itself has to be reexamined. We investigated quantitatively how much retardation is needed to retain the MMSN solid material in the disk, by deriving a formula. If the disk gas is depleted in million years, the retardation has to be twice or so. When the Jovian planet region is considered, the constraint on migration speed is more severe. The retardation has to be ~ 10. If the gas is depleted in a shorter period than the core formation time scale, it can not acquire gas to become gas giant planet. It becomes more crucial for the migration of the cores to be retarded. Such retardation can be realized by decreasing the gas to dust ratio to $\sim 1/10$ of that of MMSN, unless there is other mechanism such as turbulance to change the migration mechanism itself.

Using our formula, we can discuss how much solid material remains in specific a, if the depletion time scale is given. The formula is a function of initial gas to dust ratio and initial solid surface density. Assuming the depletion time scale is $\sim 10^6$-10^7 years, the solid material in the inner region of the disk tends to be depleted. This may be the reason for absence of planets inside Mercury ($a \sim 0.4$ AU). The disk profile is flattened by the depletion of solid material due to migration. The protoplanet disk may have had a flatter solid surface density than MMSN. Also in order for the planets to survive in the habitable zone, gas to dust ratio of the planetesimal disk has to be considerably less than that of MMSN. Such results are consistent with the planetesimal formation theory. Planetesimals can be formed more easily with small gas to dust ratio (Youdin and Shu 2002, Ishitsu and Sekiya 2003). Dust and planetesimals may have migrated to the terrestrial planet region from outer region and made the disk denser in solid material (Stevenson and Lunine 1988, Cuzzi and Zahnle 2004). If such scenario is considered, the initial planetesimal disk may have had smaller gas to dust ratio than in MMSN, which is consistent with our results. It is also possible that the monotonic inward migration time scale, which has been a serious problem in the planet formation theory, be changed from the linear theory by other mechanisms. Investigation of such mechanisms is left for future study.

Chapter 6

Appendix

6.1 Derivation of $m_{\mathrm{p,max}}(t, \Sigma_{\mathrm{S}}, a_{\mathrm{p}}), m_{\mathrm{p,max}}(\tau_{\mathrm{dep}}, \Sigma_{\mathrm{S}}, a_{\mathrm{p}})$ and $\Sigma_{\mathrm{s}}(t, a)$ with Radius Enhancement

Growth rate of a protoplanet with mass m_{p} and radius R is given by (e.g. Ida and Makino 1993),

$$\frac{\mathrm{d}m_{\mathrm{p}}}{\mathrm{d}t} = C_{\mathrm{a}}\pi\Sigma_{\mathrm{s}} f \frac{2Gm_{\mathrm{p}}R}{\langle e^2\rangle a^2 \Omega} \tag{6.1}$$

where C_{a} is a factor of a few (e.g. Ida and Nakazawa 1988,1989),
Σ_{s} is surfuce density of planetesimals, Ω is the Keplarian angular velocity ($\sqrt{GM_*/a^3}$, where M_* is the mass of the central star), f is the artificial radius enhancement, and $\langle e^2\rangle^{1/2}$ is the rms eccentricity of planetesimals. Viscous stirring by the protoplanet pumps up the eccentricity. Because we accelerate the growth of the protoplanet adopting $f = 5$, before the eccentricity is equilibriated with the damping due to the gas drag, the protoplanets grow in our simulations. Then, $\langle e^2\rangle^{1/2}$ is evaluated by equating the growth time scale τ_{growth} with the viscous stirring time scale τ_{VS}, given by (Ida and Makino 1993)

$$\tau_{\mathrm{vs}} \simeq \frac{v^3}{\pi G^2 n_{\mathrm{M}} m_{\mathrm{p}}^2 \ln\Lambda} \tag{6.2}$$

where $\ln\Lambda$ is the Coulomb logarithm which is ~ 3 (Stewart and Ida 2000), n_{M} is the number density of the protoplanets which is

$$n_{\mathrm{M}} = (2\pi ab2a\langle i^2\rangle^{1/2})^{-1} \tag{6.3}$$

and b is the separation between the protoplanets. We assume $v = v_{\rm kep}\langle e^2\rangle^{1/2}$, and $\langle e^2\rangle^{1/2} \simeq 2\langle i^2\rangle^{1/2}$. The growth time scale is expressed as $\tau_{\rm growth} = (m_{\rm p}/(dm_{\rm p}/dt))$, using eq.(6.1). Equating $\tau_{\rm growth}$ and $\tau_{\rm vs}$, the equilibrium eccentricity is

$$\langle e^2\rangle^{1/2} = 0.086 \left(\frac{\ln\Lambda}{\tilde{b} f f_{\rm ice}^2}\right)^{1/2} \left(\frac{m_{\rm p}^2\rho_{\rm p}}{\Sigma_{\rm s}^3 a^3}\right)^{1/6} \left(\frac{m_{\rm p}}{M_*}\right)^{1/3}. \tag{6.4}$$

where $\tilde{b}$ separation between the protoplanets which is normalized with $r_{\rm m,H}$ (eq.(3.8)). Integrating eq.(6.1) with eq.(6.4), we obtain

$$m_{\rm p}(t) = 1.6\times10^{-8}\left(\frac{\Sigma_{\rm s}}{\Sigma_{\rm s,SN}}\right)^2 f^2 f_{\rm ice}^2 \left(\frac{a}{1\rm AU}\right)^{-5/2}\left(\frac{\tilde{b}}{10}\right)\left(\frac{t}{1\rm year}\right) M_{\oplus}. \tag{6.5}$$

Substituting this $m_{\rm p}(t)$ into $\tau_{\rm grav,mig}$ and solve for the solid surface density, setting $\tau_{\rm grav,mig} = t$,

$$\left(\frac{\Sigma_{\rm s} f_{\rm ice}}{\Sigma_{\rm s,SN}}\right) = \frac{2.2\times10^6}{f}\left(\frac{t}{1\rm year}\right)^{-1}\left(\frac{\Sigma_{\rm g}}{\Sigma_{\rm g,SN}}\right)^{-1/2}\left(\frac{a}{1\rm AU}\right)^2 \tag{6.6}$$

where we used $\tilde{b} = 10$ and

$$c_{\rm s} = 1\times10^5\left(\frac{a}{1\rm AU}\right)^{-1/4} K. \tag{6.7}$$

for sound velocity. When $t > \tau_{\rm dep}$, $t = \tau_{\rm dep}$ is substituted in eq.(6.6) and eq.(6.5).

6.2 Derivation of $m_{\rm p,max}(t, \Sigma{\rm s}, a_{\rm p})$, $m_{\rm p,max}(\tau_{\rm dep}, \Sigma{\rm s}, a_{\rm p})$ and $\Sigma_{\rm s}(t, a)$ with No Radius Enhancement

By equating $\tau_{\rm gas}$ (2.5) and $\tau_{\rm VS}$ (6.2), the equillibrium eccentricity becomes

$$\langle e^2\rangle^{1/2} = \left(\frac{\ln\Lambda}{\tilde{b}C_{\rm D}}\right)^{1/5}\left(\frac{m_{\rm pla}\rho_{\rm p}^2}{a^3\rho_{\rm gas}^3}\right)^{1/15}\left(\frac{m_{\rm p}}{M_*}\right)^{1/3}. \tag{6.8}$$

Integrating (6.1) with (6.8), we obtain the protoplanet's mass as a function of time,

$$m_{\rm p}(t) = 10^{-18}\left(\frac{\Sigma_{\rm s} f_{\rm ice}}{\Sigma_{\rm s,SN}}\right)^3\left(\frac{a}{1\rm AU}\right)^{-81/10}\left(\frac{\rho_{\rm p}}{3{\rm gcm}^{-3}}\right)^{-1/5}\left(\frac{m_{\rm pla}}{10^{20}{\rm g}}\right)^{-2/5}\left(\frac{\tilde{b}}{10}\right)^{6/5}\left(\frac{\Sigma_{\rm g}}{\Sigma_{\rm g,SN}}\right)^{6/5}\left(\frac{t}{1\rm year}\right)^3 M \tag{6.9}$$

assuming $C_\mathrm{D} = 0.5$ and $M_* = M_\odot$. Substituting (6.9) into $\tau_{\mathrm{grav,mig}}$ and solve for the solid surface density,

$$\left(\frac{\Sigma_\mathrm{s} f_\mathrm{ice}}{\Sigma_\mathrm{s,SN}}\right) = 4\times10^7 \left(\frac{t}{1\mathrm{year}}\right)^{-4/3} \left(\frac{\Sigma_\mathrm{g}}{\Sigma_\mathrm{g,SN}}\right)^{-11/15} \left(\frac{a}{1\mathrm{AU}}\right)^{16/5} \left(\frac{\rho_\mathrm{p}}{3\mathrm{gcm}^{-3}}\right)^{1/15} \left(\frac{m_\mathrm{pla}}{10^{20}\mathrm{g}}\right)^{2/15} \left(\frac{\tilde{b}}{10}\right)^{-2/5}. \tag{6.10}$$

Bibliography

[1] Adachi, I.,C. Hayashi, and K. Nakazawa 1976. The gas drag effect on the elliptical motion of a solid body in the primordial solar nebula. *Prog. Theor. Phys.*,**56**,1756-1771.

[2] Agnor, C. B., R. M. Canup, and H. F. Levison 1999. On the character and consequences of large impacts in the late stage of terrestrial planet formation. *Icarus*,**142**,219-237.

[3] Agnor, C. B., and Ward, W. R. 2002. Damping of terrestrial-planet eccentricities by density-wave interactions with a remnant gas disk. *ApJ*,**567**,579-586.

[4] Artymowicz, P. 1993. Disk-satellite interacton via density wave and the eccentricity evolution of bodies embedded in disks. *A.J.*,**419**,166-180.

[5] Artymowicz, P. 1994. Orbital Evolution of Bodies Crossing Disks Due to Density and Bending Wave Excitation *ApJ*,**423**,581.

[6] Barge, P., and R. Pellat 1991. Mass spectrum and velocity dispersion during planetesimal accumullation. I. Accretion. *Icarus*,**93**,270-287.

[7] Chambers, J. E., and G. W. Wetherill 1998. Making the terrestrial planets: N-body integrations of planetary enbryos in three dimensions. *Icarus*,**136**,304-327.

[8] Cuzzi, J. N. and K. J. Zahnle 2004. Material Enhancement in Protoplanetary Nebulae by Particle Drift through Evaporation Fronts *ApJ*,**614**,490-496

[9] Goldreich,P., and S. Tremaine 1979. The excitation of density waves at the Lindblad and corotation resonances by an external potential *ApJ*,**233**,857-871

[10] Goldreich,P., and S. Tremaine 1980. Disk-satellite interactions *ApJ*,**241**,425-441

[11] Gomes, R. S., A. Morbidelli and H. F. Levison 2004. Planetary migration in a planetesimal disk: why did Neptune stop at 30 AU? *Icarus*,**170**,492-507.

[12] Greenberg, R., J. Wacker, W. K. Hartmann, and C. R. Chapman 1978. Planetesimals to planets: Numerical simulations and collisional evolution. *Icarus*,**35**,1-26.

[13] Greenzweig, Y. and J. J. Lissauer 1992. Accretion rates of protoplanets. II - Gaussian distributions of planetesimal velocities *Icarus*,**100**,440-463.

[14] Haisch, K. E. Jr., E. A. Lada and C. J. Lada 2001. Disk Frequencies and Lifetimes in Young Clusters *ApJ*,**553**,L153-L156.

[15] Hayashi, C., K. Nakazawa and I. Adachi 1977. Long-Term Behavior of Planetesimals and the Formation of the Planets *PASJ*,**29**,163-196.

[16] Hayashi, C. 1981. Structure of the solar nebula, growth and decay of magnetic fields and effects of magnetic and turbulent viscosities on the nebula. *Prog. Theor. Phys. Suppl.*,**70**,35-53.

[17] Hayashi, C. & K. Nakazawa, and Y. Nakagawa, 1985. Formation of solar system *Protostars and planets*,**II**,1100-1153.

[18] Ida, S. & J. Makino 1993. Scattering of planetesimals by a protoplanet: Slowing down of runaway growth. *Icarus*,**106**,210-227.

[19] Ida, S. & K. Nakazawa 1989. Collisional probability of planetesimals revolving in the solar gravitational field. III *A&A*,**224**,303-315.

[20] Ida, S., G. Bryden, D. N. C. Lin and H. Tanaka 2000. Orbital Migration of Neptune and Orbital Distribution of Trans-Neptunian Objects *ApJ*,**534**,428-445.

[21] Inaba, S., H. Tanaka, K. Nakazawa, G. W. Wetherill, and E. Kokubo 2001. High-accuracy statistical simulation of planetary accretion: II. Comparison with N-body simulation. *Icarus*,**149**,235-250.

[22] Inaba, S., G. W. Wetherill, and M. Ikoma 2003. Formation of gas giant planets: core accretion models with fragmentation and planetary envelope *Icarus*,**166**,46-62.

[23] Ishitsu, N. and M. Sekiya 2003. The effects of the tidal force on shear instabilities in the dust layer of the solar nebula *Icarus*,**165**,181-194.

[24] Kasting, J. F., D. P. Whitmire and R. T. Reynolds 1993. Habitable Zones around Main Sequence Stars *Icarus*,**101**,108-128.

[25] Kokubo, E., and S. Ida 1995. Orbital evolution of protoplanets embedded in a swarm of planetesimals. *Icarus*,**114**,247-257.

[26] Kokubo, E., and S. Ida 1996. On runaway growth of planetesimals. *Icarus*,**123**,180-191.

[27] Kokubo, E., and S. Ida 1998. Oligarchic growth of protoplanets. *Icarus*,**131**,171-178.

[28] Kokubo, E., and S. Ida 2000. Formation of protoplanets from planetesimals in the solar nebula. *Icarus*,**143**,15-27.

[29] Kokubo, E., and S. Ida 2002. Formatioin of Protoplanet Systems and Diversity of Planetary Systems. *ApJ*,**581**,666-680.

[30] Kominami, J., and S. Ida 2002. The effect of tidal interaction with a gas disk on formation of terrestrial planets. *Icarus*,**157**,43-56

[31] Kominami, J., and S. Ida 2004. Formation of terrestrial planets in a dissipating gas disk with Jupiter and Saturn *Icarus*,**167**,231-243

[32] Korycansky, D. G. and J. B. Pollack 1993. Numerical calculations of the linear response of a gaseous disk to a protoplanet *Icarus*,**102**,150-165

[33] Laughlin, G., A. Steinacker, F.C. Adams 2004. Type I planetary migration with MHD turbulence *ApJ*,**608**,489-496

[34] Lin, D. N. C., and J. Papaloizou 1985. On the dynamical origin of the solar system. *Protostars and planets***II**,981-1072.

[35] Makino, J. 1991. Optimal order and time-step criterion for Aarseth-type N-body intergrators. *ApJ*,**369**,200-212.

[36] Makino, J., and S. J. Aarseth 1992. On a hermite integrator with Ahmad-Cohen scheme for gravitational many-body problems. *PASJ*,**44**,141-151.

[37] Nelson, R. P. and J. C. B. Papaloizou 2004. The interaction of giant planets with a disc with MHD turbulence - IV. Migration rates of embedded protoplanets *MNRAS*,**350**,849-864

[38] Ohtsuki, K., S. Ida, Y. Nakagawa, K. Nakazawa 1993. Planetary accretion in the solar gravitational field. *Protostars and Planets III*,**A93-42937 17-90**,1089-1107

[39] Shu, Frank H., C. Yuan and J. J. Lissauer 1983. Nonlinear Density Waves in Saturn's Rings *Bulletin of the American Astronomical Society*,**15**,959.

[40] Spaute, D., S. Weideschilling, D. R. Davis, and F. Marzari 1991. Accretional evolution of a planetesimal swarm: I. A new simulation. *Icarus*,**92**,147-164.

[41] Stevenson D. J. and J. I. Lunine 1988. Rapid formation of Jupiter by diffuse redistribution of water vapor in the solar nebula *Icarus*,**75**,146-155.

[42] Stewart, G. R., and S. Ida 2000. Velocity Evolution of Planetesimals: Unified Analytical Formulas and Comparisons with N-Body Simulations *Icarus*,**143**,28-44.

[43] Tanaka, H., and S. Ida 1996. Distribution of Planetesimals around a Protoplanet in the Nebula Gas *Icarus*,**120**,371-386.

[44] Tanaka, H., and S. Ida 1999. Growth of migrating protoplanet. *Icarus*,**139**,350-366.

[45] Tanaka, H., T. Takeuchi and W. R. Ward 2002. Three-Dimensional Interaction between a Planet and an Isothermal Gaseous Disk. I. Corotation and Lindblad Torques and Planet Migration *ApJ*,**565**,1257-1274.

[46] Tanaka, H. and W. R. Ward 2004. Three-dimensional Interaction between a Planet and an Isothermal Gaseous Disk. II. Eccentricity Waves and Bending Waves *ApJ*,**602**,388-395.

[47] Ward, W. R. 1986. Density waves in the solar nebula - Differential Lindblad torque *Icarus*,**67**,164-180

[48] Ward, W. R. 1988. On disk-planet interactions and orbital eccentricities *Icarus*,**73**,330-348

[49] Ward, W. R. 1993. Density Wave In The Solar Nebula: Planetesimal Velocities. *Icarus*,**106**,274-287.

[50] Ward, W. R. 1997. Protoplanet migration by nebula tides *Icarus*,**126**,261-281

[51] Ward, W. R. and J. M. Hahn 1994. Damping of orbital inclinations by bending waves *Icarus*,**110**,95-108

[52] Ward, W. R. and J. M. Hahn 1995. Disk tides and accretion runaway. *ApJ*,**440**,L25-L28

[53] Weidenschilling, S. J.,D. Spaute, D. R. Davis, F. Marzari, and K. Ohtsuki 1997. Accretional evolution of a planetesimal swarm. 2. The terrestrial zone *Icarus*,**128**,429-455.

[54] Wetherill, G. W. and S. R. Stewart 1989. Accumulation of a swarm of small planetesimals. *Icarus*,**77**,330-357.

[55] Wetherill, G. W. and S. R. Stewart 1993. Formation of planetary embryos - Effects of fragmentation, low relative velocity, and independent variation of eccentricity and inclination *Icarus*,**106**,190-209.

[56] Youdin, A. N. and F. H. Shu 2002. Planetesimal Formation by Gravitational Instability *ApJ*,**580**,494-505.

Acknowledgement

I would like to thank Dr. S. Ida and Dr. H. Tanaka for scientific guidance. A successful completion of this thesis would not be possible without them. Most of the simulations were carried out using the host computers and GRAPE-6A in TITech. Support from Dr. H. Emori in using the computers has been a great help on this thesis. I would also like to thank Dr. H. Daisaka for advising me on the N-body code. Some of the simulations were performed on the computers in MUV in NAOJ.

Discussions with Dr. D. Lin improved this study greatly. He gave us new ideas and insights concerning this study. Significant improvement was accomplished in workshops and conferences. I thank Dr. T. Guillot and Dr. R. Sari for comments on the gas depltion mechanism and time scales. I appreciate Dr. S. Watanabe, Dr. T. Nakamoto, Dr. E. Kokubo, Dr. M. Ikoma and Dr. S. Inaba for fruitful comments. This work is supported by JSPS Research Fellowship.